

Fuselage Structure Optimisation

Stéphane Grihon

AIRBUS, Toulouse, France

Manuel Samuelides, Antoine Merval[‡]

ONERA, Toulouse, France

Alain Remouchamps, Michael Bruyneel, Benoit Colson

SAMTECH, Liège, Belgium

Klaus Hertel

AIRBUS, Bremen, Germany

Nomenclature

STIFFOPT	= Stiffened Panel Optimisation
NLFEA	= Nonlinear Finite Element Analysis
HPC	= High Performance Computing
CFRP	= Carbon Fibre Reinforced Plastic
MSE	= Mean Squared Error
PHP	= Hypertext Preprocessor
σ	= Stress
σ_{all}	= Stress allowable
RF	= Reserve Factor
GFEM	= Global Finite Element Model
λ	= Sizing design variables
$W(\lambda)$	= Weight function
IL [*]	= Fixed internal loads
IL(λ)	= Updated internal loads
PL	= Local optimisation problem
PG	= Global optimisation problem
PLL	= Local optimisation problem
sh	= Stringer height
wt	= Web thickness
wh	= Web height
ffw	= Free flange width
fft	= Free flange thickness
aft	= Attached flange thickness
afw	= Attached flange width
st	= Skin thickness
pt	= Pad thickness
pw	= Pad width
p	= Stringer pitch
rp	= Rivet pitch
DC, D _{fast}	= Diameter of fasteners: continuous value
PB	= Post-buckling margin

[‡] PhD student

D_{next}

= Catalog value and next in catalog

RF_{stat}	= Reserve factor for static strength
RF_{RS}	= Reserve factor for residual strength
σ_{max}	= Maximum stress
$\sigma_I, \sigma_{II}, \sigma_{VM}$	= Minor, major principle and Von Mises stresses
$E_{skin}, E_{stringer}, E_{frame}$	= Young modulus of skin, stringer, frame
ν	= Poisson ratio
$S_{skin}, S_{stringer}, S_{frame}$	= Section areas of skin, stringer, frame
N_{xx}, N_{yy}, N_{xy}	= Fluxes
F_{XSR}	= Longitudinal force in the super-stringer
$RF_{fatXRaid}, RF_{fatXSkin}, RF_{fatYSkin}$	= Fatigue reserve factors
M_Y	= Bending moment in the fuselage section
$v=Z-Z_G$	= Vertical distance with respect to the center of gravity
I	= Quadratic moment of the fuselage section
DoE	= Design of Experiments
NN	= Neural Network
MoE	= Mixture of Experts
LHC	= Latin Hyper Cube
$t_{angle}^{SKIN,i}$	= Skin thickness variables (composite panel use-case)
$t_{angle}^{STRINGER,i}$	= Stringer thickness variables (composite panel use-case)
λ	= Loading factor for buckling and non-linear analysis

Abstract

An optimization framework dedicated to stiffened panel optimization (STIFFOPT) has been implemented and demonstrated on aircraft fuselage covers. The framework incorporates three methodologies, which have been developed with consideration of the design stage:

- In rapid sizing approaches the optimization is based on design curves obtained from the approximation of local optimization results using surrogate models (Neural Nets). Another solution would have been to approximate the analysis results (Reserve Factors) with surrogate models, but it was found too tedious regarding the large dimension of the input space. Finally a capability has been developed to accelerate the design process with design curves. The latter gives the minimum cross sectional area of a structural element for given internal loads and can be interrogated in place of local optimization processes, either interactively by designers who need recommendations for optimum solutions, or directly, via in-house software tools like STIFFOPT in order to automate the sizing of wider structures.
- In preliminary sizing approaches the optimization is based on exact stress responses obtained from semi-analytical stress tools. The selected approach is built upon independent local optimizations. Even if not fully optimal in terms of internal load redistribution and design continuity, the proposed approach has the advantage of being very easy to parallelize with the possibility to launch every structural element optimization on an independent processor.
- In detailed sizing approaches the optimization is based on advanced stress responses obtained either from semi-analytical stress tools or from non-linear finite element analysis (buckling/post-buckling) for which a gradient-based optimization approach has been developed. Few publications demonstrate such a capability. Key

developments have been made to guarantee the robustness of the optimization process, both with respect to linear buckling and with respect to non-linear post-buckling. All structural responses have been differentiated and their sensitivities have been obtained through the application of a semi-analytical approach. An adequate formulation of the post-buckling optimization problem has been established. A robust capability is now ready for post-buckling optimization of composite stiffened panels based on detailed finite element analysis.

High-Performance Computing (PC cluster) has been used to ensure reasonable computational times. This approach is particularly important to the last stage of the design (i.e., detailed sizing based on nonlinear finite element analysis).

I. Introduction

A. Preamble

The application of numerical optimization to engineering design was introduced several decades ago starting with structural optimization.¹ Since then, structural optimization has always been at the root of multidisciplinary optimization and today is a major component of Multidisciplinary Design Optimization (MDO). The algorithms developed for structural optimization are fairly generic and therefore can be very useful to MDO, especially those regarding multi-level optimization as discussed in this chapter.

B. Context

The aeronautical industry is a business governed by increasing customer demands for product performance, cost and time-to-market reduction. Numerical optimisation, in turn, is a key technology to achieve these goals due to the successful marriage of:

- mathematical theories and associated algorithms which guarantee an optimum performance and
- advanced software, which facilitates the automation and integration of the design lifecycle and thus ensures reduction of lead times²⁻⁴

In this context the trends for business globalisation together with advances in massively parallel IT solutions and the worldwide web encourage structural design to adopt distributed computing concepts.^{5,6} This is the notion of extended enterprise, discussed in more detail in the chapter dedicated to the virtual enterprise. In order to fulfil these requirements a modular multi-step process for optimisation of structural covers has been implemented. The basic idea was to fully map the manual sizing process.

C. Sizing process

Since aircraft structures are made of thin shells working essentially as membranes, buckling strength must be taken in consideration. This is also the reason why longitudinal beams called stiffeners are added to the shell.⁷ Such an arrangement is known as the stiffened panel concept, which is generally used for airframe covers (see figure).

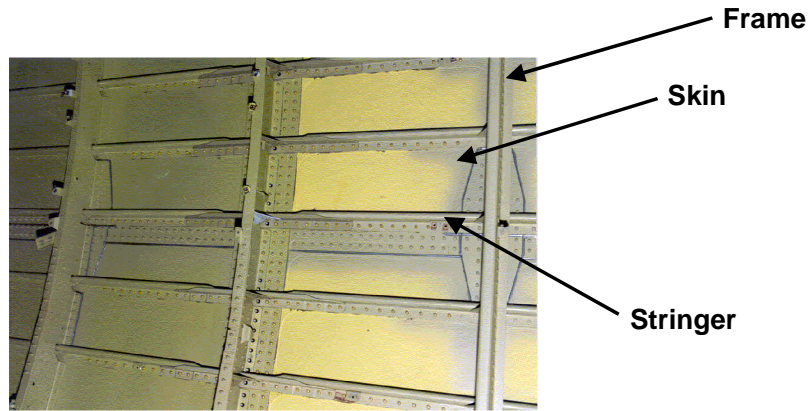


Fig.1: The stiffened panel concept

Moreover for local analysis needs, each stiffened panel is decomposed into panel bays also called super-stiffeners, as depicted in figure 2. Hence the super-stiffener appears as the elementary pattern for the hand-made stress and sizing process of airframe covers.

Of course isolating a super-stiffener to analyse the stability of covers assumes that the buckling/post-buckling is localised: this is generally a good approximation if a suitable transverse stiffening is provided (e.g, orbital frames for a fuselage structure).

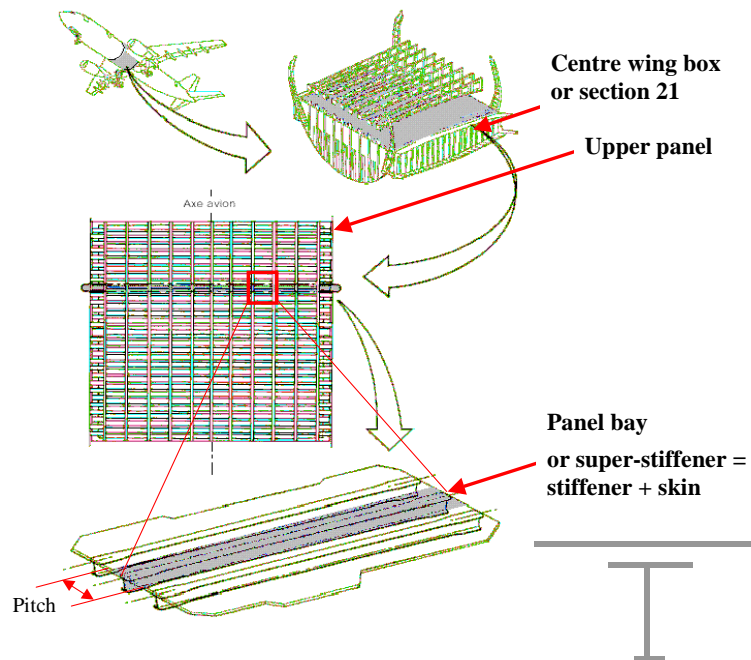


Fig.2: Airframe structure decomposition

The advantage of such an approach is that the sizing process is decomposed down to a very fine level of granularity allowing a very flexible implementation of optimisation methods.

Thus the super-stiffeners are generally computed with standard stress tools, which are analytically based, including engineering methods relying on handbook formulae, test data banks and experience.

The local analysis uses internal loads extracted from a GFEM (Global Finite Element Model) after a static linear analysis based on external loads. Specific post-processing tools have to be used in order to compute a loading adapted to the super-stiffener model, see figure 3.

The local analysis delivers RFs (Reserve Factors).

A Reserve Factor is a value greater than 1 if the structure is feasible. For example, if σ_{all} is the failure stress for a given material, the Reserve Factor is the ratio $\frac{\sigma_{all}}{\sigma}$, where σ is the current stress value.

For buckling/post-buckling, the RFs include the RF for skin buckling and the RF for super-stringer collapse (column collapse).

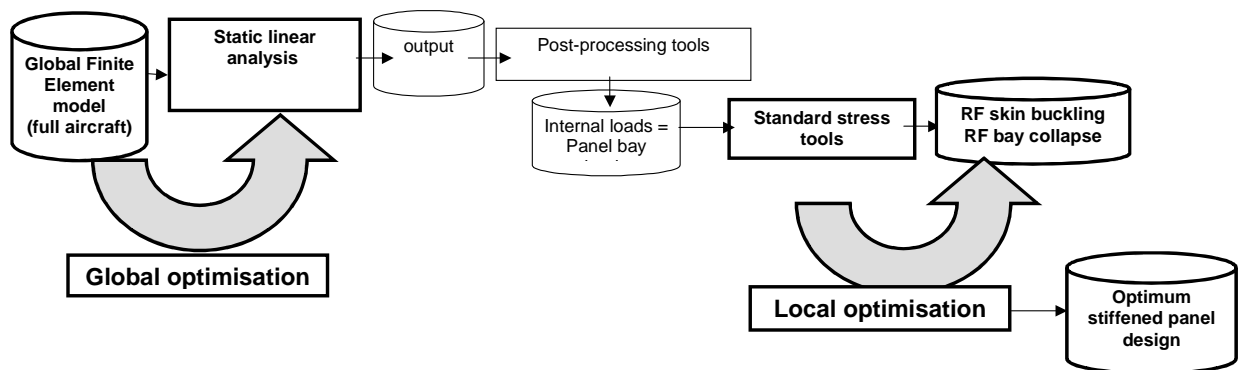


Fig.3 : Design & stress process / global-local analysis & optimisation link

Hence the current design and stress process for a fuselage structure is a bi-level one with global and local analyses.

D. Selection of an optimisation process

In the same way, the optimisation can be viewed as a local or a global optimisation.

Local optimisation integrates local analysis and is based on fixed internal loads.

The local optimisation problem solved (P_L) is the following one:

$$(P_L) \begin{cases} \text{Min } W(\lambda) \\ RF(\lambda, IL^*) \geq 1. \end{cases}$$

IL^* : fixed internal loads

with

- λ : sizing design variables (skin thickness and stringer section parameters)
- $W(\lambda)$: weight objective function
- $RF(\lambda; IL^*)$: reserve factor as function of sizing variables and internal loads

Global optimisation integrates global analysis and is based on updated internal loads. The global optimisation problem solved is the following one:

$$(P_G) \begin{cases} \text{Min } W(\lambda) \\ RF(\lambda, IL(\lambda)) \geq 1. \end{cases}$$

$IL(\lambda)$: updated internal loads

To be properly solved this formulation requires to compute internal load sensitivities and to combine with RF sensitivities (chain ruling). This is feasible but complex. This process has been implemented since this research work at AIRBUS.²⁷ But it is complex and heavy and cannot yet be used for a full structure sizing.

The position of this research work was more to reflect the manual sizing process, while keeping simplicity and modularity to make easier distributed computing approaches, knowing that it is not fully optimum. This manual sizing process consists in sizing each super-stringer independently with fixed internal loads. The corresponding optimisation scheme is then local optimisation. However, this local optimisation is done with fixed internal loads, while it is clear that changing the sizing also changes the stiffness hence the distribution of internal loads. The internal load redistribution is generally considered further in the design when a new GFEM is built. No systematic convergence is searched for.

Thus the optimisation and quality of optimisation results is only guaranteed after longer term loops (FE and load loops of an aircraft project) have been performed. The purpose here is to go one step further and to iterate the internal load updates up to convergence.

Hence the algorithm used is the following one:

- Step1: update the GFEM with new sizing properties λ_k**
- Step2: compute new internal loads IL_k**
- Step3: solve PL with $IL^*=IL_k$: gives λ_{k+1}**
- Step4: $\lambda_k \leftarrow \lambda_{k+1}$**
- Step5: Go to Step1 while significant variation of λ and/or IL**

With this approach, the first objective is then to integrate this sizing process, that is, to integrate the super-stiffener optimisation capability in the global design and stress process. Starting from super-stiffener optimisation, as the main brick, a capability is built for full panel optimisation, considering internal load redistribution based on GFEM updates and static re-analyses.

The rest of the chapter is organised as follows:

In section 2, the case study used in this work is introduced.

In section 3, the implementation of a local optimisation session for a typical super-stiffener is presented then demonstrated on a set of super-stiffeners

In section 4, the integration of the STIFFOPT software is described.

In section 5, a tight coupling integration is presented. The demonstration is first made on a set of panels. Then a full fuselage barrel is optimised, using a PC cluster.

In section 6, a loose coupling scenario is explored based on design curves built with local optimisations and neural networks.

In section 7, some complements to the sizing process are discussed.

In section 8, a refinement of the local optimisation process is proposed based on non-linear finite element analysis of the super-stiffener.

II. Presentation of the test-case

The test-case used for all method comparisons and validations consists in a fuselage barrel of a very large civil transport aircraft. This barrel is located between the left cargo door and the wing, more exactly between frame 38 and frame 46, as depicted in figure 4.

There are 8 frames in orbital direction and 146 stiffeners in longitudinal direction.

The zone contains consequently 1168 stiffeners.

50 load cases were used for the sizing optimisation but an envelope was made (commented in section 4).

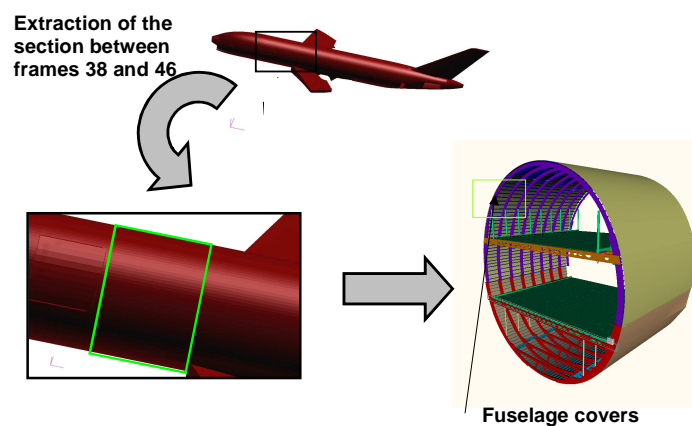


Fig.4 : Fuselage barrel test-case

III. Local optimisation

The purpose of this section is to present and demonstrate the main brick of the optimisation process: the local super-stringer optimisation.

A. Definition

As described before the purpose of the local optimisation is to solve the following problem:

$$\left(P_L \right) \begin{cases} \text{Min } W(\lambda) \\ \text{RF}(\lambda, \mathbf{IL}^*) \geq 1. \end{cases}$$

\mathbf{IL}^* : *fixed internal loads*

The exact instantiation for this local optimisation problem and a more physical description are presented below.

1. Design principle

The design principle selected for the use-case is the following one:

- material: metallic (isotropic aluminium)
- stringer section: Z-shape, see figure 5.

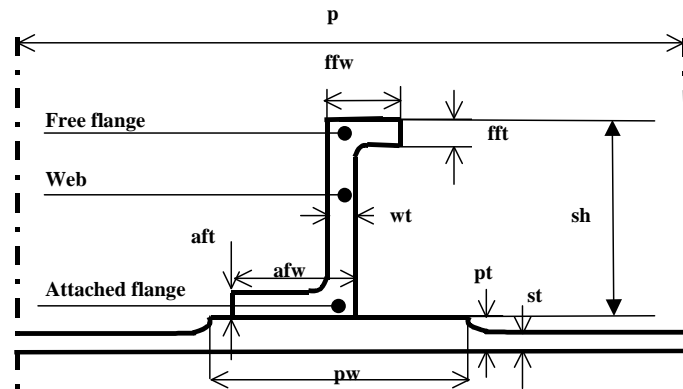


Fig.5 : Design variables for a Z-shaped stringer profile

2. Stress hypotheses and criteria

Specific computations are considered to compute internal loads from the direct output of the GFEM (NASTRAN static linear analysis - SOL101).⁸

Specific stress allowables are considered to take into account fatigue and damage tolerance. For stability a skill tool is used: ASSIST.⁹ ASSIST implements engineering formulae to analyse buckling/post-buckling of stiffened panels based on a super-stringer pattern. The post-buckling behaviour is considered up to collapse considering also material plasticity.

3. Objective function

As the targeted fuselage section use-case has got a uniform frame pitch and material, optimising the weight is equivalent to optimising the cross sectional area of each super-stringer.

For this reason the objective function is the cross sectional area of the super-stringer.

4. Design variables

The six following variables are considered within the given bounds (all sizes in mm):

Stringer height (sh)	$25.<sh<55.$
Web stringer thickness (wt)	$1.6<wt<4.$
Free flange width (ffw)	$8.<ffw<26.$
Free flange thickness (fft)	$2.<fft<4.$
Attached flanged thickness (aft)	$1.6<aft<4.$
Skin thickness (st)	$1.6<st<8.$

The super-stiffener section area is computed with these variables. The attached flange width (afw) and pad thickness (pt) values are linked with skin thickness. Pitch (p) has not been selected as a design variable. It is possible to give some indications of optimum pitch values based on a local optimisation. However it should be mixed with a parameterised GFEM to be able to change the pitch. This will be considered in a future work.

5. Design constraints

A number of six design constraints allow to have a geometry conveying designer experience and to avoid discontinuity in super-stiffener geometry. The range of each constraint is set by designer experience and must be respected at the end of the local optimisation process.

3 aspect ratios (width/height to thickness ratios) are used to control the geometry (please refer to figure 5 for the definition of the various sizes):

$$3. < \frac{afw}{aft} < 20.$$
$$3. < \frac{sh - fft - aft}{wt} < 20.$$
$$3. < \frac{ffw}{fft} < 10.$$

Two thickness ratios between each stringer dimensions:

$$\frac{aft}{wt} > 1.3$$
$$\frac{aft}{st} > 1.3$$

Attached flange width must be twice greater than free flange width in order to avoid a too long free flange:

$$\frac{afw}{ffw} > 2.$$

Inequality constraints linked to fastener installation and pad are considered as active, that is, satisfied as equalities. This is based on experience from previous stiffened panel optimisation studies and allows reducing the number of design variables by explicit relations. The width of the attached flange is given by the free edge distance and the minimum distance to the web. The attached flange width is thus linked to diameter and web thickness (4 is the fillet radius).

$$afw = 2. * D_{fast} + \frac{D_{next}}{2.} + wt + 4.$$

D_{fast} and D_{next} are the fastener diameter and the following diameter in a given catalog:

$$D_{fast} \text{ and } D_{next} \in \{4.; 4.8; 5.6; 6.4; 8. \}$$

Pad width is linked to attached flange width

$$pw = 2. * (3. + \frac{afw}{2.})$$

Pad thickness is linked to skin thickness only :

$$pt = 1.4 * st$$

The fastener pitch is taken as 4.5 times the diameter.

$$rp = 4.5 * D_{fast}$$

D_{fast} and D_{next} are discrete values computed using DC.

DC is the continuous version of the fastener diameter.

DC=0.5*(aft+1.4*st) following the rule of the total fastened thickness.

Then DC is round-off to D_{fast} using the following staired function :

$$D_{fast} = 4 + 0.8 * f(DC - 4) + 0.8 * f(DC - 4.8) + 0.8 * f(DC - 5.6) + 1.6 * f(DC - 6.4),$$

where f is a function defined $f(x) = (1 + \text{sign}(x))/2$

6. Physical constraints

Buckling:

If $st \leq 3$, $PB \geq 60$

If $3 \leq st \leq 5$, $PB \geq 80$

If $st \geq 5$, $PB \geq 100$

These three conditions build a margin policy for buckling on-set: depending on the skin thickness, the skin is authorised to buckle at a certain percentage PB of limit loads.

To implement this step rule, the same principle as for diameter is used:

$$(PB)_{min} = 60 + 20 * f(st - 3) + 20 * f(st - 5) \text{ with } f(x) = (1 + \text{sign}(x))/2.$$

The reserve factor for collapse is computed by ASSIST and incorporates the effect of local stringer buckling.

Static strength :

$$RF_{stat} = \frac{\sigma_{all}}{\sigma_{max}}, \quad \sigma_{max} = \max(\sigma_I, \sigma_{II}, \sigma_{VM})$$

Residual strength:

$$RF_{RS} = \frac{\sigma_1 * \left(\frac{E_{frame} * S_{frame}}{E_{frame} * S_{frame} + E_{skin} * S_{skin}} \right) + \sigma_2}{N_{yy} \text{ tenue} / \text{Skin}_{thickness}}$$

with

- E: Young modulus of each structural element
- S: Section area of each structural element
- N_{yy} : orbital flux
- σ_1, σ_2 : values based on experience

This allowable was built by fatigue specialists and is based on tests for various panels and gives the stress allowable as a function of the orbital stiffening ratio.

Crack initiation in the stringer:

$$RF_{fatXStringer} = \frac{\sigma_{all}}{\frac{F_{XSRfat} * E_{Stringer}}{E_{Stringer} * S_{Stringer} + E_{Skin} * S_{Skin}} - \frac{F_{Poisson}}{S_{Stringer}}}$$

with

- F: longitudinal force
- $F_{Poisson}$: further commented

Crack growth in the skin:

$$RF_{fatXSkin} = \frac{\sigma_{all}}{\frac{F_{XSRfat} * E_{Skin}}{E_{Stringer} * S_{Stringer} + E_{Skin} * S_{Skin}} + \frac{F_{Poisson}}{S_{Skin}}}$$

Crack growth in the stringer:

$$RF_{fatYSkin} = \frac{\sigma_{all}}{N_{YYfat} / st}$$

Crack initiation in the skin does not appear because it is covered by crack initiation in the stiffener.

When there is a stress in longitudinal direction, the skin tends also to be deformed in the orbital direction due to the Poisson effect.

$$F_{Poisson} = \frac{\nu}{st} * \frac{E_{Stringer} * S_{Stringer} * S_{Skin}}{E_{Stringer} * S_{Stringer} + E_{Skin} * S_{Skin}} * N_{yy}$$

All these formulae take into account a local redistribution of internal loads between the skin and stringer. This is necessary because stringer and skin dimensions vary along the optimisation.

Depending on the criterion considered, specific load cases are used:

- static ultimate loads for strength (limit loads for residual strength)

- reference fatigue load cases for crack initiation and propagation

The optimisation problem finally consists in minimising the super-stringer cross-sectional area based on the above-mentioned design variables and taking into account:

- design variable bounds (box constraints)
- (explicit) links between design variables
- implicit links between design variables: design constraints
- structure feasibility constraints: $RF \geq 1$, also called physical constraints

The mathematical programme is easy to write (based on this summary) and is not shown here for brevity.

B. Implementation

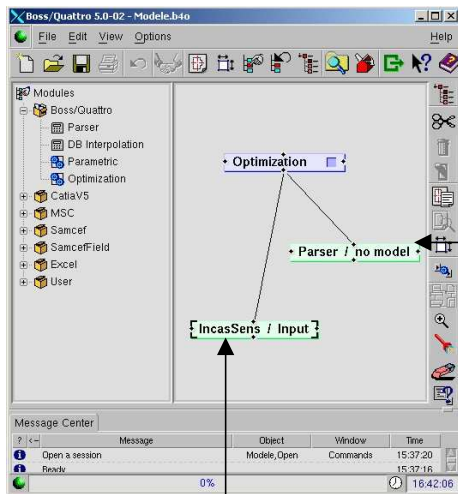
The purpose is to build a local optimisation process embedding

- constraints based on simple equations
- constraints based on the output of complex programmes (skill tools) and especially the ASSIST stability analysis tool

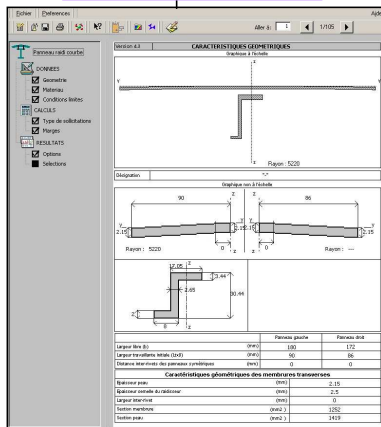
Rather than writing the interface with a mathematical library like NAG¹⁰ or NASTRAN it was decided to use a software framework dedicated to integration of external software for easy and fast integration and to benefit from a Graphic User Interface. BOSS Quattro from SAMTECH company was used for that purpose.²⁻⁴

Integrating an external tool, identifying design variables and results to be constrained or optimised is rather simple with an optimisation framework as depicted in Figure 6. Moreover BOSS Quattro's library of algorithms was found quite satisfactory for solving the complex optimisation problem defined before, considering also the non-linear behaviour of the responses as well as the singularities introduced (stair functions for diameter for example).^{11,12}

GUI to integrate the optimisation process

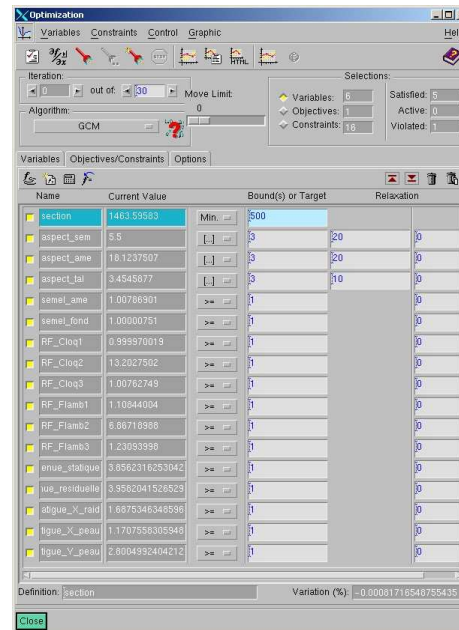


ASSIST software



Explicit equation

$$RF_{RS} = \frac{368,75 * \left(\frac{E_{frame} * S_{frame}}{E_{frame} * S_{frame} + E_{skin} * S_{skin}} \right) + 8,4375}{N_{yy} \text{tenu} / \text{Skin}_{thickness}}$$



GUI to manage design variables and responses (objective and constraints)

Fig.6: Local optimisation integration

A practical implementation is worth noticing: as the framework interfaces external applications through files and as sensitivities are computed with finite differences (small perturbations: see figure 7 for illustration), it was found preferable to compute sensitivities externally (figure 8).

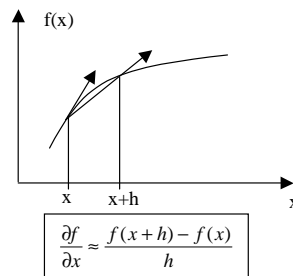


Fig.7: Principle of finite difference sensitivity analysis

The reason for that was not least due to the benefit, which can be gained from the ASSIST implementation. That is, a list of geometries (as well as a list of load cases) can be given as input and analyses are iterated inside the tool without re-initialisation and additional input/output times. This approach gives much smaller computational times than doing computations separately.

Considering that the relative step for sensitivities is $h=10^{-3}$, the following geometry table is given as input to ASSIST.

This approach is appealing because it is in accord with the zero order algorithms, which calculate one population at each iteration.

sh	wt	ffw	fft	aft	st
sh*(1+10 ⁻³)	wt	ffw	fft	aft	st
sh	wt*(1+10 ⁻³)	ffw	fft	aft	st
sh	wt	ffw*(1+10 ⁻³)	fft	aft	st
sh	wt	ffw	fft*(1+10 ⁻³)	aft	st
sh	wt	ffw	fft	aft*(1+10 ⁻³)	st
sh	wt	ffw	fft	aft	st*(1+10 ⁻³)

Fig.8: Table of geometries to be computed for current analysis and computation of sensitivities

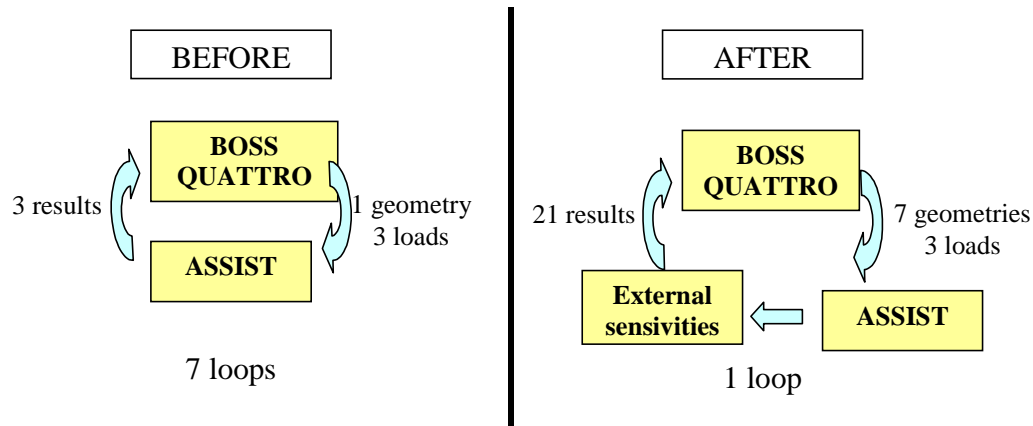


Fig.9: Principle for implementation of sensitivity analysis

The time savings estimated for such an implementation above are about 60%: an iteration now takes 15 s compared with 40 s before parametric use. The main reason for this lower time is the reduction of file input/output obtained through externalisation of the finite difference calculations as illustrated in the figure 9.

C. Demonstration on a set of super-stringers

1. Test-case

To check and demonstrate local optimisation, a set of 5 super-stringers was selected across the barrel in the frame bay between frame 42 and frame 43. Figure 10 illustrates the location of these super-stringers.

In an actual detailed design all 72 super stringers will be calculated. This is to be doubled to consider the other half-barrel. Then top and lower stringers (S0 and S73), lying in the symmetry plan, have to be added. A total of 146 super-stringers is thus to be considered for the full frame bay.

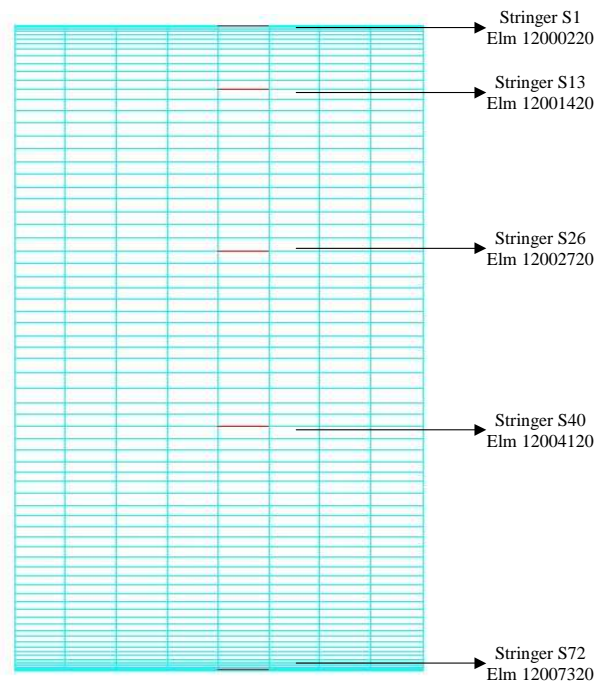


Fig.10: Principle for implementation of sensitivity analysis

2. Optimum section areas

Figure 11 shows the section areas found for the super-stringers at convergence:

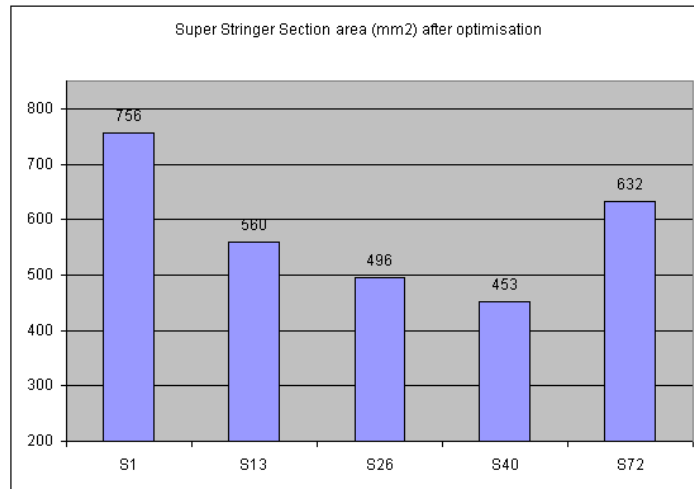


Fig.11 Super-stringer section areas after optimisation

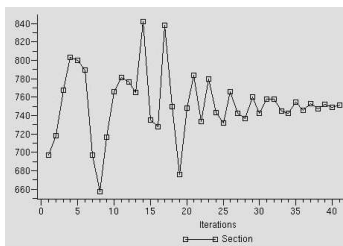
They are consistent with the loading of the super-stringers: a high compression force results in a super-stringer with a large section area. For example, Stringer 1 supports 106116 N as compression force while only 23514 N for stringer 26 (Fig. 12).

Stresses	S1	S13	S26	S40	S72
Super stringer max compression force (N)	-106 116	-46 561	-23 514	-20 499	-116 670
Static super stringer force (N)	184 267	84 989	21 222	35 686	39 273
Fatigue super stringer force (N)	58 563	27 943	21 294	14 733	6 289

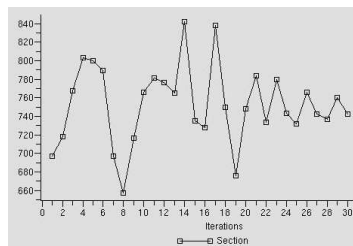
Fig.12: Super-stringer loading

Remark: The super-stringer S1 has a larger section than S72 while a lower compression load, because the fatigue load is more important.

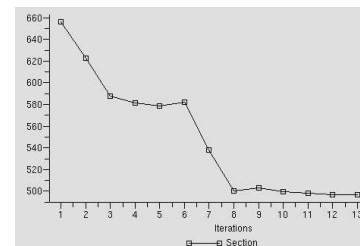
3. Convergence history



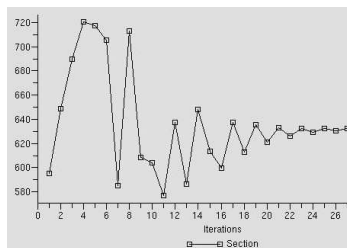
S1: 39 iterations



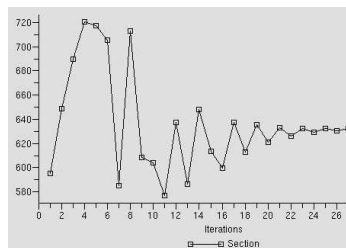
S13: 28 iterations



S26: 13 iterations



S40: 23 iterations



S72: 27 iterations

Stringer number	S1	S13	S26	S40	S72
Iteration number	39	28	13	23	27

Fig.12: Optimisation histories

The convergence is difficult because of the non-linearity of ASSIST: sometimes the responses are known to be non-differentiable. This is the reason why the convergence histories appear chaotic and sometimes quite long.

Nevertheless, the optimisation histories show a convergence in less than 40 iterations. Also looking at convergence plots in Figure 12, it seems that the convergence can be truncated at about 30 iterations. This is a good lesson learnt: as several cycles linked to internal load updates are performed, it is possible to truncate the convergence in order to have smaller computational times. This principle is applied further to the STIFFOPT process discussed below.

4. Stringer profiles

Web height is high when a super-stiffener with large section (heavily loaded) must be designed (Stringer S1 and S72). Indeed, web height is known as the main driver for the column collapse RF.

Free flange and attached flange thickness are always larger than web thickness. Free flange width is less than attached flange width because of a specific design constraint added.

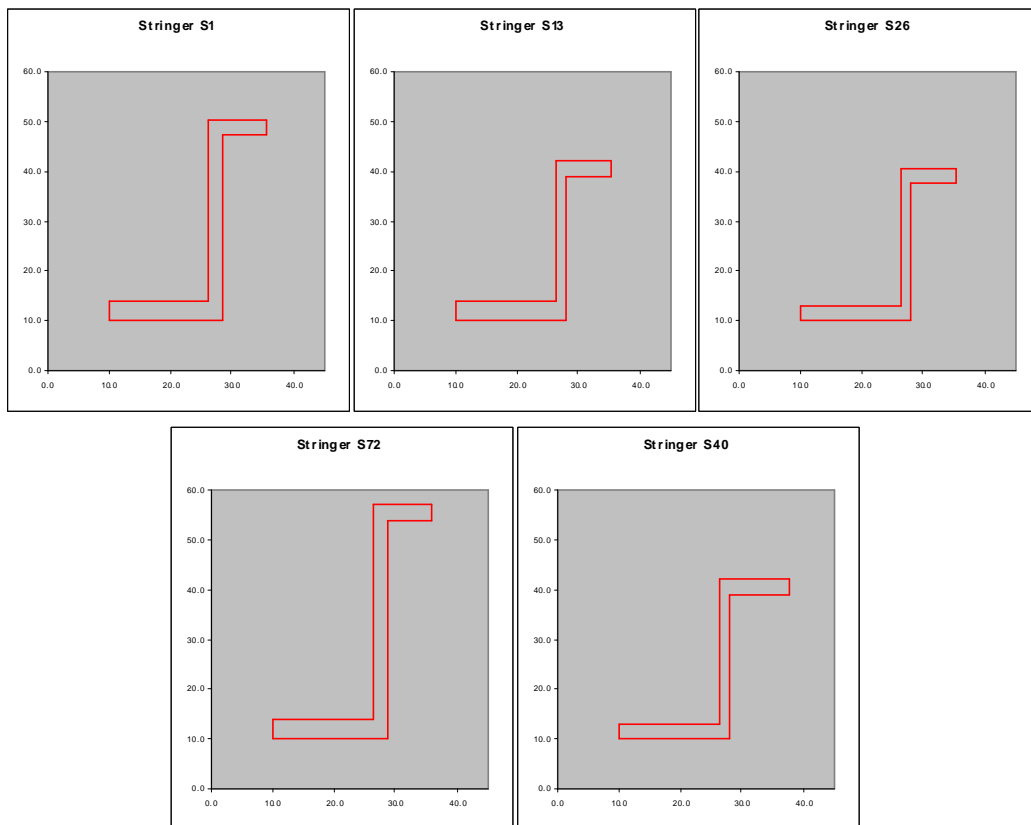


Fig.13: Optimum stringer profiles

This demonstration shows that the local optimisation behaviour is correct and in agreement with the designer experience.

The next step of integration can then be initiated.

IV. Integration

A. The STIFFOPT framework

1. STIFFOPT Principle

The principle of STIFFOPT is to integrate the local optimisation process validated and demonstrated previously in a wider environment in order to implement the algorithm presented in the introduction.

This supposes a mechanism able to:

- initialise the sizing
- prepare all local optimisation sessions
- launch all local optimisations
- collect all sizing results after completion of these optimisations
- update GFEM properties
- run a new linear static analysis with this updated GFEM
- post-process the internal loads including a load envelope
- launch a new optimisation based on the previous sizing results

As the GFEM is compliant with the NASTRAN format and as part of the process requires to update GFEM properties, PATRAN was considered as necessary in the process. Moreover PATRAN offers a Graphical User Interface (GUI) and authorises customisation thanks to its internal command language PCL.¹³ PATRAN can also be used to launch NASTRAN analysis such as SOL101 linear static analysis.

PATRAN can also be adapted to launch other processes such as local optimisations.

Finally the integration is based on three Commercial Off The Shelf (COTS) tools: as shown in Figure 14. It also integrates the Airbus in-house tool ASSIST.

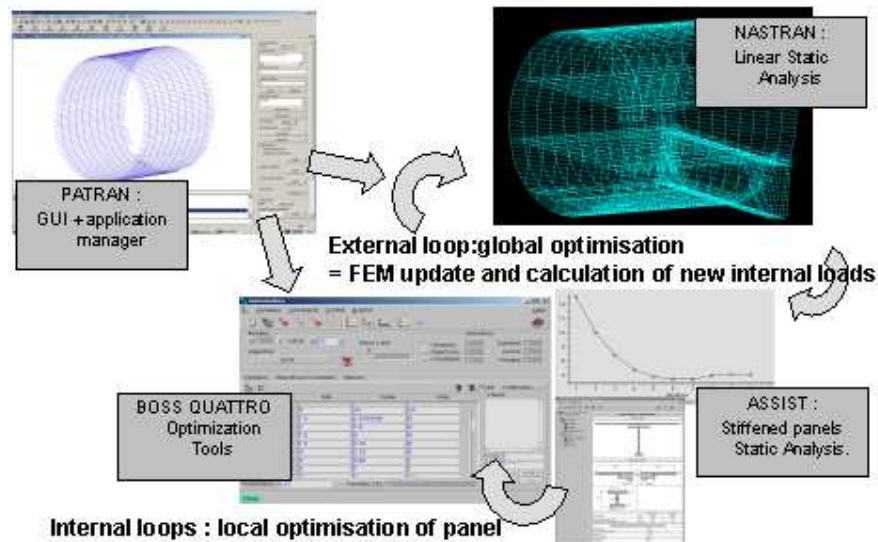
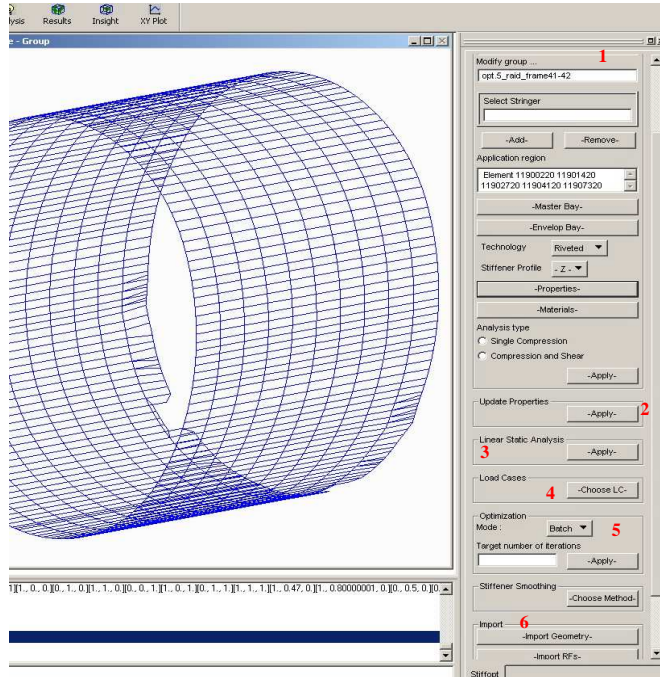


Fig.14 STIFFOPT Principle and COTS used

Moreover PATRAN pre-processing capabilities allow defining the region of interest: the set of super-stringers to be optimised. It is also possible to define groups of super-stringers having the same sizing properties to simplify and reduce the size of the problem. This is further described below.

2. STIFFOPT GUI

The STIFFOPT process is displayed in a vertical menu of the PATRAN main window. Figure 15 presents this menu and the associated steps of the process.



1 - Users create stiffener groups with properties for the first loop → **Group Definition**

2 - GFEM is updated with stringer geometry since the 2nd loop is done → **Update Properties**

3 - Internal load redistribution is computed using the new GFEM → **Linear Static Analysis**

4 - Users choose static and fatigue load cases → **Load cases**

5 - Envelope computing is made with new internal load redistribution and optimization is launched → **Optimisation**

6 - Results are imported in order to set new geometry in stiffener group → **Import**

Fig.15 STIFFOPT vertical menu and successive steps

Remark: Every second loop necessarily begins with new geometry updating in order to guarantee the consistency of the finite element results with the current definition of stringer bays.

Step 1: Group definition

Super-stiffener groups are set during this step. Properties and materials are selected for each group. A group can be either created, modified or deleted.

The “modify” option enables the user to change the current design as he wishes and without any specific interaction with the process (except a slower convergence if the design is changed too much with respect to the final optimum results). This option can be very important in the final stage to smooth the design in order to achieve a continuous variation of stringer dimensions (constant height for example). Some tools have been developed to help this manual process.

Master bay and envelope bay methods are optional.

They allow grouping super-stringers and reducing the number of optimisations to be performed for computational time reasons:

- The “Master bay” approach consists in attributing the sizing obtained for one super-stringer to all super-stringers of a group

- The “Envelope bay” approach consists in optimising a theoretical super-stringer with an envelope of internal loads computed over the full group. Then the sizing of this theoretical super-stringer is attributed to all super-stringers of the group.

All super-stringers are optimised independently in the default option.

Technology and stringer shape are then chosen. A riveted stringer with a “Z” shape is the only choice for the time being, but “I” and “J” shape will be set in future versions. Optimisation sessions are already available from past applications.

Figure 16 illustrates the three ways exist to input properties:

- manually by writing in the listbox “value” with possibility to copy one sheet to the others for repetitive properties
- using directly ASSIST GUI by clicking on the “Assist” button to get a graphical reference for properties
- importing an existing ASSIST file by clicking on the “Import” button for data already available

Of course it is possible to copy-paste the information for one stringer to the other ones to limit the input effort. Materials are then to be chosen from a given list for skins, stringers and frames.

The last step is to choose ASSIST computation type. “Single compression” is chosen if the study zone is not significantly loaded with shear. “Compression and shear” is the default choice.

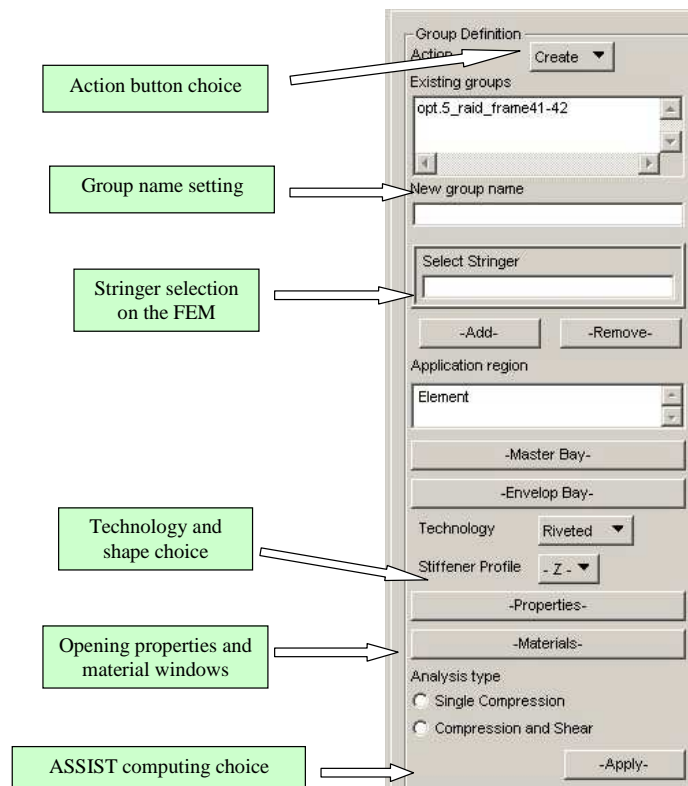


Fig.16: STIFFOPT - definition of super-stringer groups

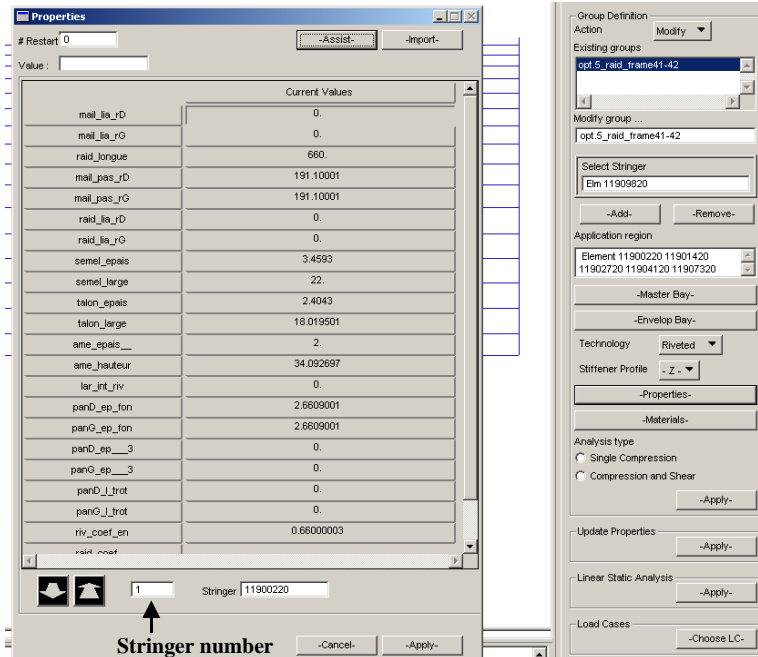


Fig.17: Input of properties

Steps 2 to 4: Update properties, Linear Static Analysis and Load Cases

“Update Properties” see figure 17 allows to set new properties of stringer in the GFEM. The GFEM is updated with stringer and skin section area computed with new properties (web height, free flange thickness, etc).

Stringer properties come from results of the last optimisation loop or from properties setting.

Since the GFEM geometry has been modified, a linear static analysis SOL 101 must be launched.⁸ This analysis gives new load redistribution of internal loads. Analysis steps are as following as shown in Figure 18:

- a *.blk file is created when users click on “Apply”.
- a *.xdb is obtained after running NASTRAN.
- A *.xdb file is attached by users on the GFEM.

At least, “Load Case” button opens a window where users choose static and fatigue load cases. These selections are used for linear static analysis and for envelope computing.

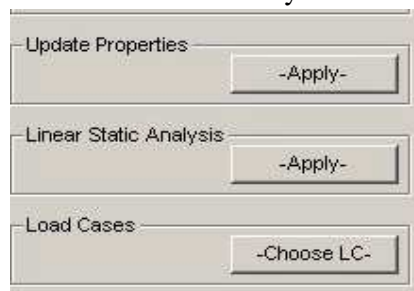


Fig.18 : Management of global analysis

Step 5: Envelope computing & Optimisation

Before launching optimization, 3 files must be created for each stringer and put in a repository:

- a BOSS QUATTRO session file *.b4o
- an Assist file *.ses
- a neutral file *.in

Figure 20 shows how These files are set in a repository tree composed of groups and stringers.

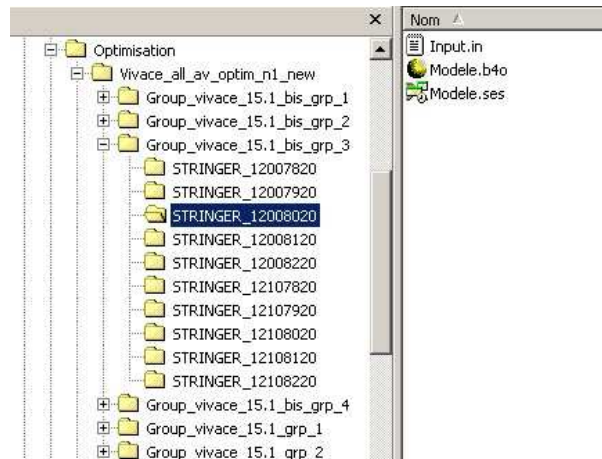


Fig.19 : Management of optimisation data

The files are created by PCL using an envelope approach for internal loads in order to obtain sizing constraints values. Envelope computing for each super-stringer is consequently done using a new load redistribution of internal loads and chosen load cases.

The longitudinal force in the stringer F_x and three fluxes in the skin (N_{xx} , N_{yy} and N_{xy}) are taken from linear static analysis results for each stringer bay.

The structural responses (see section 3) are computed using these 4 results for each stringer during a loop on selected load cases:

- Maximum bay compression force (sum of the force in the stringer and adjacent skin fluxes multiplied by half -itches) and associated shear (direct stress output)
- Maximum shear and associated compression force
- Compression force and associated shear for maximum principle stress
- Maximum force for static load cases
- Flux N_{yy} for static load cases
- Maximum force for fatigue load cases
- Maximum force for fatigue load cases centred on the skin (sum of flux in the skin multiplied by pitch and half-forces in adjacent stringers)
- Flux N_{yy} on the skin for fatigue load cases

To launch the optimisation the user can then choose “batch” or “interactive” modes:

- batch : optimisation session files are set and the optimization is launched
- interactive : optimisation session files are only set and the optimisation is not launched

The maximum number of iterations can be manually set if the users wish to accept an incomplete convergence.

Finally, users click on “Apply” button (Figure 20) and optimization is launched.

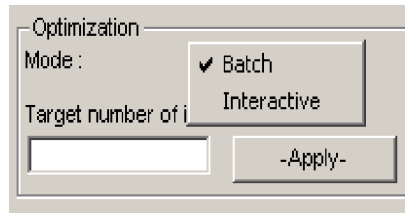


Fig.20: Management of the optimisation process

Step 6: Import

At the end of the optimization, 3 actions can be performed (Fig. 21):

- 1 - Setting new geometry in stringer properties → Import Geometry
- 2 - Show buckling Reserve Factor in an array → Import RFs
- 3 - Show mass for each stringer in an array → Import Mass

When the user clicks on “Import Geometry”, each stringer repository is cleared and only the final files are preserved (modele_end.b4o and input.in for example). Each stringer geometry is set in a file named modele.txt. This file is read and new properties values are set in each properties stringer array.



Fig.21: Management of optimisation results

B. Demonstration on a single panel

To validate the convergence of the global optimisation process with update of internal loads, a preliminary test case was performed on a limited zone (4 stringer bays have been optimized in panel 15.7). A fast convergence of sizing was observed. Then a more extensive test-case has been solved as explained below.

The optimisation was performed for 72 stringer bays located in an area between frames 42 and 46 and stringers 0 to 21 for the panels 15.1 and 15.2 as depicted in Figure 22.

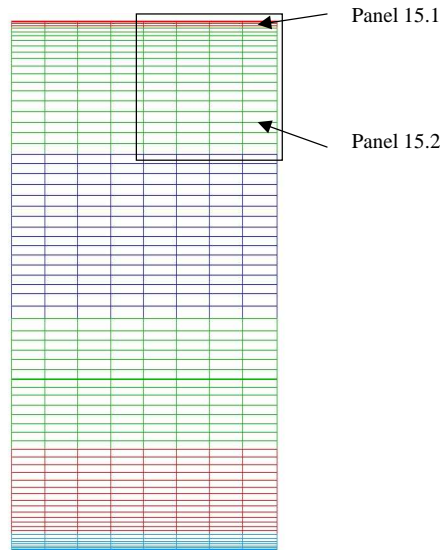


Fig.22 : Management of optimisation results

The initial sizing of the stringers is the same and is consistent with the finite element properties.

- Initial stringer section area= 114.24mm² (same for the GFEM)
- Initial stringer bay section area = 661.24mm² (for the GFEM stringer bay = 650mm²)

For the set of optimised stringer bays, a fast convergence has once again been observed. The dimensions are stabilised after three global iterations. As Figure 23 shows, some convergence oscillations can be observed around limit values and the convergence is non-monotonic as already observed for local optimisation test-cases.

Stringer bay section areas are :

- increased in the upper part of the fuselage
 - o Str 1 : final stringer section = 163.5mm², final stringer bay section = 713.6mm²
- decreased in the lateral part
 - o Str 15 : final stringer section = 135.8mm², final stringer bay section = 597.9mm²

This evolution is given as an example for three stringer bays in Fig.23 below.

The variation along the iterations of maximum compression forces is surveyed in order to evaluate the internal load redistribution. In addition to the stringers whose dimensions are controlled (Str 1, 5, 10, 15 et 20), gauge stringers are used to investigate the variations of internal loads far from the optimised region. These are stringers 21, 31 and 41 for the inter-frames 43-44 and 44-45.

The variation of internal loads for the optimised stringer bays 1, 10 and 20 and for the gauge stringer bays 0, 21,31 and 41 is reported in Fig.23.

		init	1optim	2optim	3optim	4optim	5optim
Str 1	aft	4	2,618	2,62	2,618	2,618	2,618
	afw	10	23,782	23,798	23,782	23,782	23,782
	fft	1,6	1,817	1,929	1,818	1,819	1,876
	fiw	24	18,874	19,188	16,151	15,042	15,197
	wt_	1,6	2,182	2,198	2,182	2,182	2,182
	wh	22,4	31,972	32,966	32,727	32,727	32,727
	st	2,75	2,724	2,695	2,711	2,689	2,702
	tt	3,5	3,814	3,773	3,795	3,764	3,782
	pw	14,5	14,51	14,52	14,53	14,51	14,51
S Str	114,24	166,318238	171,82368	163,034108	161,032988	162,181162	
S StrBay	650,365	702,418138	702,22124	712,336148	705,828488	709,604762	
Str 10	aft	4	2,618	2,618	2,618	2,618	2,618
	afw	10	23,782	23,782	23,782	23,782	23,782
	fft	1,6	1,821	1,818	1,818	1,818	1,818
	fiw	24	15,901	9,841	9,839	9,79	9,827
	wt_	1,6	2,182	2,182	2,181	2,181	2,182
	wh	22,4	25	28,161	28,149	27,707	28,038
	st	2,75	2,275	2,295	2,295	2,266	2,288
	tt	3,5	3,185	3,213	3,213	3,172	3,203
	pw	14,5	14,51	14,51	14,51	14,51	14,51
S Str	114,24	145,766997	141,599516	141,541547	140,488463	141,305678	
S StrBay	650,365	593,496097	593,264696	606,526907	599,586583	604,866978	
Str 20	aft	4	2,618	2,618	2,618	2,618	2,618
	afw	10	23,782	23,782	23,782	23,782	23,782
	fft	1,6	1,818	1,818	1,818	1,818	1,818
	fiw	24	9,476	9,472	9,472	9,544	9,472
	wt_	1,6	2,182	2,182	2,182	2,182	2,182
	wh	22,4	25	25	25	25,598	25
	st	2,75	2,1	2,09	2,09	2,166	2,1
	tt	3,5	2,941	2,926	2,927	3,032	2,941
	pw	14,5	14,51	14,51	14,51	14,51	14,51

Fig.23 : Variation of 4 stringer bay dimensions
Str 1, 10 and 20, Fr 43-44.

Some dimensions reach rapidly a common final value for all stringers. This is due to the activation of several design constraints linking these dimensions as described in section 3.1. This shows that these constraints have probably to be relaxed and/or improved to get real optimum sections for the stringers.

		init	1 optim	2 optim
Str 0	Fx StrBay	-99964	-98286	-98062
Str 1	Fx StrBay	-98365	-96630	-96753
	Fx Str	-23784	-23808	-24611
Str 10	Fx StrBay	-57888	-59126	-59008
	Fx Str	-11515	-14730	-14256
Str 20	Fx StrBay	-37747	-37179	-37159
	Fx Str	-7936	-9158	-9147
Str 21	Fx StrBay	-33730	-32961	-33049
Str 31	Fx StrBay	-12970	-12908	-12922
Str 41	Fx StrBay	23946	23956	23952

Fig.24 : Evolution of internal loads for 3 optimised stringer bays (Str 1, 10 et 20) and for 4 gauge stringer bays (Str 0, 21, 31, 41) ;Fr 43-44.

The above figure 24 shows :

- A large variation of internal loads after the first optimisation then a smaller variation showing that the optimisation process is rapidly stabilised. Beyond the 2nd optimisation there is no real variation of dimensions hence internal load variations have not been estimated
- A significant reduction of internal loads (absolute value) in the upper part of the fuselage where the stringer bay sections are increased.
- An increase of internal loads in the lateral part where the stringer bay section is decreased
- A little variation of internal loads in the gauge stringer bays

Attempts to clearly explain the impact of sizing variations on the internal loads are difficult because there are both section increase and decrease in the region.

Considering the beam theory explained in more detail in the dedicated chapter on aeroelasticity and sizing in a multi-level modelling approach for pre-design, the distribution of axial loads in the fuselage section is governed by the equation :

$$F_{XSR} = \sigma.S = \frac{M_Y}{I} . v.S$$

where:

M_Y : bending moment for the whole fuselage section,

I : quadratic moment of inertia for the fuselage section,

$v = z-z_G$: vertical distance from the section centre of gravity to the considered stringer bay position.

So the evolution of axial forces is a combination of global variations, (I, z_G) variations and local section variations. Moreover, the same analysis should be made in the y-axis for a lateral bending moment included in the set of sizing load cases (lateral gust).

Hence accurate computations should be done to justify clearly the behaviour of internal loads.

Altogether, this first case of validation is encouraging giving a rapid convergence to the STIFFOPT process but must be now widely extended. Indeed the area optimised is still limited and thus the impact of sizing changes on the distribution of internal loads are also rather limited. To make a more convincing test-case it is necessary to work on a full fuselage section. This is the purpose of the next section.

V. Tight coupling

The tight coupling process is investigated in this section. The tight coupling consists in direct calls to the stress tool ASSIST inside the local optimisations. The tight coupling is defined in opposition with the loose coupling described in section 6. The loose coupling process consists in replacing the local optimisations based on ASSIST with the use of surrogate models. These surrogate models are Artificial Neural Networks built from intensive local optimisations performed a priori, before using STIFFOPT.

A. High Performance Computing (HPC) implementation

1. Why HPC is necessary and easy to implement ?

Computational times are very heavy for the optimisation of a full use-case. Despite some potential time savings arising from:

- external sensitivity analysis in the local optimisations,
- reduction of load cases based on an envelope,
- optional use of master bay and envelope bay methods,

super-stringer per super-stringer optimisation can take a very long time.

If STIFFOPT optimises the zone between frame 38 and 46, 1168 local optimisation session files must be launched (1168 stands for 8 inter-frames times $2*72+2=146$ stringers per inter-frame: top and lower specific stringers have not been optimised in the symmetry plan).

Since one iteration lasts 15s and about 15 iterations are necessary to reach convergence, one stringer optimisation lasts about 4 min.

An optimization with 1168 stringers will last about 80 hours.

Nevertheless one large advantage of the approach selected is its inherent parallelism: each super-stringer optimisation is independent from the other ones.

Hence a natural and direct way of reducing computational times is to perform each optimisation on a separate processor.

Of course 1168 processors are not necessarily available. So, at least, what can be done is to group computations in equal size sets and send each set to a separate processor.

2. Computational means

A demonstration of such a process was made based on standard desk PCs.

A set of 30 PCs was used over night to parallelise computations.

Figure 16 shows how The network is composed of 30 workstations Dell Precision that are used each day. Computation grid is consequently available only during the night.

The technical characteristics are the following:

- workstations Dell Precision 360
- Processors PIV 2.5 – 3.2 Ghz
- 512 Mo and 2Go of DDR SDRAM
- [80-120] Go disk (IDE & SATA)
- Video board Quadro4 and Quadro Fx.

3. PC Grid principle

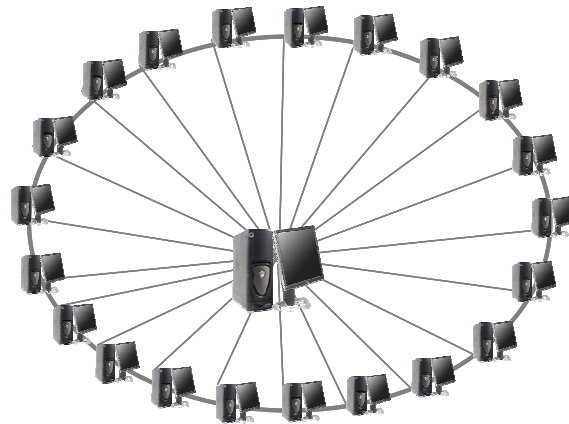


Fig.25 PC Grid principle illustration

The Grid computing method is composed of 4 steps as illustrated on Fig.26:

- 1 - Boss Quattro files are created on a master workstation
- 2 - The master workstation dispatches one file for each slave workstation
- 3 - Optimisation is launched on slave workstation
- 4 - Result files are imported to master workstation after optimization

The theoretical speed-up factor is consequently the number of PC. The practical speed-up factor is very close to the theoretical speed-up factor.

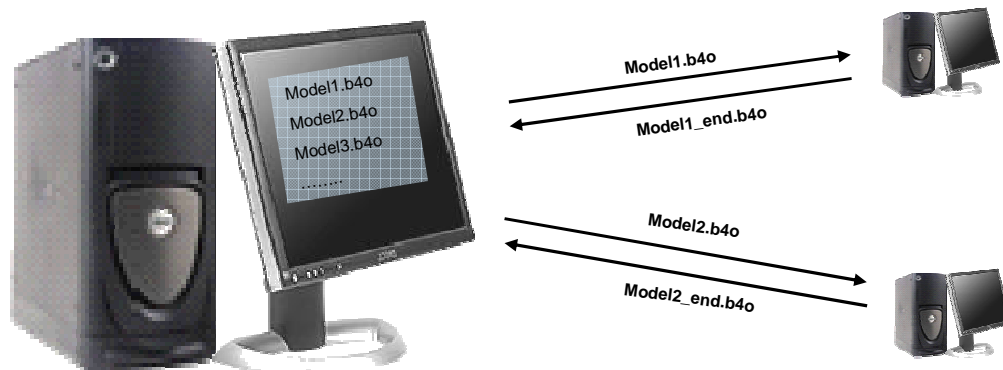


Fig.26 Grid computing principle

If grid computing is used with 30 workstations, computation time is reduced by a factor closed to 30: 3hours versus 80hours as shown in figure 28.

4. Management of the parallel process

A GUI in PHP: Hypertext Preprocessor (PHP) programming language has been created to launch computation grid.^{14,15}

The steps are:

- 1 - process initialisation
- 2 - census of available PC
- 3 - census of session file available
- 4 - process launch

This program is launched with the master workstation as shown on Fig.27.



The screenshot shows a GUI window titled "Menu Principal". The menu is divided into two sections: "Initialisation" and "Calcul".

- Initialisation:** Remise à zéro, Machines disponibles, Recensement des mailles
- Calcul:** Lancement du processus, Force Check, Avancement et statistiques, Arrêter le processus

Below the menu is a table with the following data:

Machine	Maille	Calcul	Transfert	Itérations
mhoarau	Group_vivace_15.1_bis_grp_1/STRINGER_11607820/	121 s	1 s	0
elemenach	Group_vivace_15.1_bis_grp_1/STRINGER_11607920/	60 s	1 s	0
fhopp	Group_vivace_15.1_bis_grp_1/STRINGER_11608020/	122 s	1 s	0
slesaint	Group_vivace_15.1_bis_grp_1/STRINGER_11608120/	-	0 s	0
nkawski	Group_vivace_15.1_bis_grp_1/STRINGER_11608220/	123 s	1 s	0
gschlosser	Group_vivace_15.1_bis_grp_1/STRINGER_11707820/	124 s	1 s	0
melduayen	Group_vivace_15.1_bis_grp_1/STRINGER_11707920/	125 s	0 s	0
...

Fig.27 Management of the parallel process

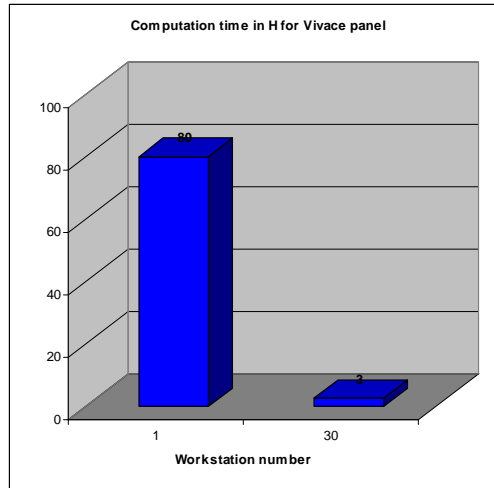


Fig.28 Computation time with grid computing

With such an HPC approach, we can now imagine a full fuselage optimisation. We have, however, focused our demonstration on the fuselage barrel test-case, which is now possible to optimise in a “reasonable” time.

B. Demonstration for a full barrel

48 groups of super-stiffeners were set. But in each group the optimisation has been performed super-stringer per super-stringer.

12 panels exist in the section (6 each side of the fuselage) and each panel is divided into four groups.

- group 1 : frame 38-40
- group 2 : frame 40-42
- group 3 : frame 42-44
- group 4 : frame 44-46

The following Fig.29 gives the 48 group names. They follow the physical panelisation as illustrated on Fig.22.

Panels	Group 1	Group 2	Group 3	Group 4
15.1	15.1_grp_1	15.1_grp_2	15.1_grp_3	15.1_grp_4
15.1_bis	15.1_bis_bis_grp_1	15.1_bis_bis_grp_2	15.1_bis_bis_grp_3	15.1_bis_bis_grp_4
15.2	15.2_grp_1	15.2_grp_2	15.2_grp_3	15.2_grp_4
15.2 bis	15.2_bis_bis_grp_1	15.2_bis_bis_grp_2	15.2_bis_bis_grp_3	15.2_bis_bis_grp_4
15.3	15.3_grp_1	15.3_grp_2	15.3_grp_3	15.3_grp_4
15.3 bis	15.3_bis_bis_grp_1	15.3_bis_bis_grp_2	15.3_bis_bis_grp_3	15.3_bis_bis_grp_4
15.34	15.34_grp_1	15.34_grp_2	15.34_grp_3	15.34_grp_4
15.34 bis	15.34_bis_bis_grp_1	15.34_bis_bis_grp_2	15.34_bis_bis_grp_3	15.34_bis_bis_grp_4
15.42	15.42_grp_1	15.42_grp_2	15.42_grp_3	15.42_grp_4
15.42 bis	15.42_bis_bis_grp_1	15.42_bis_bis_grp_2	15.42_bis_bis_grp_3	15.42_bis_bis_grp_4
15.46	15.46_grp_1	15.46_grp_2	15.46_grp_3	15.46_grp_4
15.46 bis	15.46_bis_bis_grp_1	15.46_bis_bis_grp_2	15.46_bis_bis_grp_3	15.46_bis_bis_grp_4

Fig.29 Topology of groups

The results provided in Figure 30 show 4 optimisation loops were computed because the convergence is fast. Indeed, the convergence is reached after loop 2 when the gap percentage is only 0.23%.

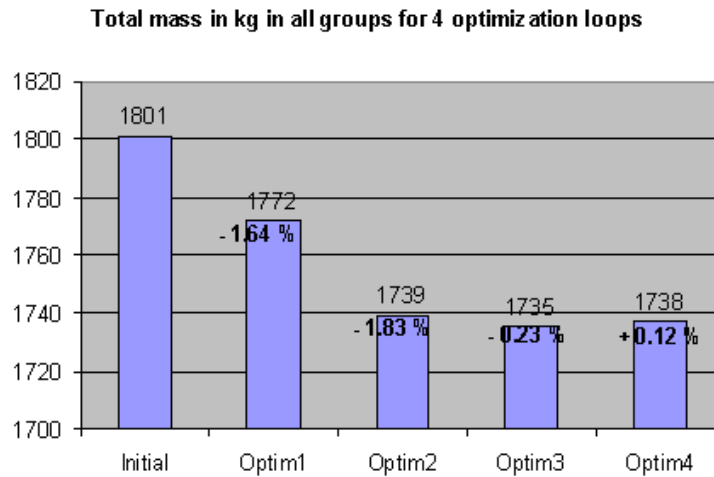


Fig.30 Convergence history of the full section mass

Results are analysed panel per panel and not per group. There are 12 panels.

Figures 31 and 32 show gap percentages between each optimisation for each group.

The panel convergence is not homogenous. Two convergence cases exist:

- Case 1 : 9 panels

Since the initial constraints are not active, the initial mass is too great and mass decreases with optimization. The gap percentage between optimisation is always negative and reaches zero.

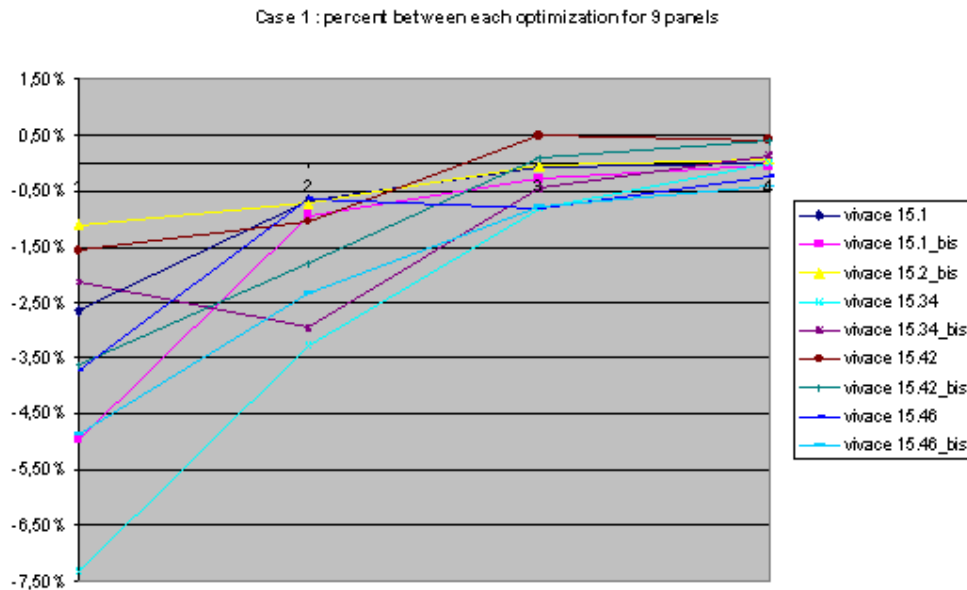


Fig.31. Convergence of Case 1

- Case 2: 3 panels

Since some initial constraints are active or violated, mass increases after optimization 1 to permit constraints to be allowable. Then the problem is the same as case 1 for optimisation 2. The gap percent is first positive and then negative. Finally, it reaches zero. That means the stringer is optimal.

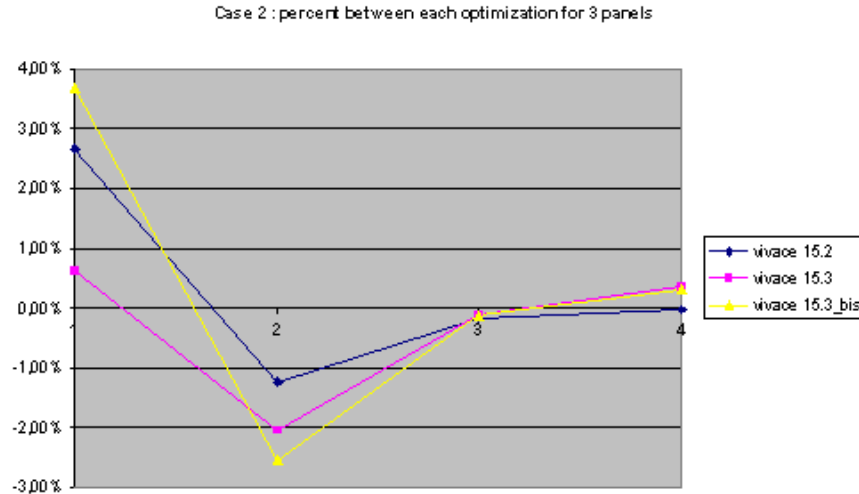


Fig.32 Convergence of Case 2

The Figure 33 shows the mass of each panel for the four optimisation loops.

The mass of panel 15.2, 15.3 and 15.3_bis increases after the first loop. The panels that are in the middle top of the fuselage are close to the optimum. Indeed, initial mass and mass after the last loop is almost the same.

The mass of panels 15.1, 15.1_bis, 15.46 and 15.46_bis does not decrease a lot. Since these panels correspond to zones which support strong stresses (top and bottom of the fuselage), the optimisation does not give an important decreasing of mass.

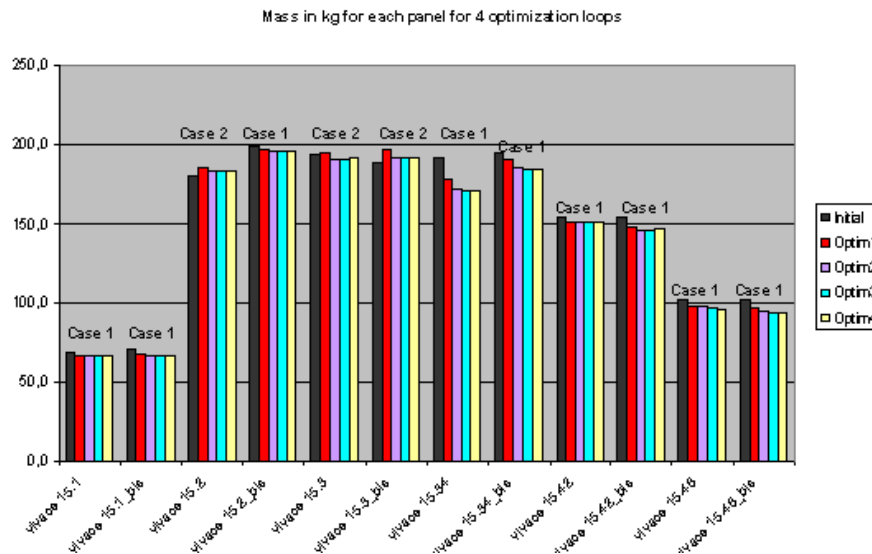


Fig.33 Convergence history panel per panel

Stiffener Number	Frame 38-39 Frame 39-40 Frame 40-41 Frame 41-42 Frame 42-43 Frame 43-44 Frame 44-46 Frame 46-46								Panel
	116	117	118	119	120	121	122	123	
2	725.12	705.17	687.93	680.04	676.54	673.92	672.15	671.27	
3	793.05	701.08	680.23	672.48	667.96	665.80	664.73	662.48	
4	801.25	687.69	669.82	660.02	656.36	655.19	655.00	654.52	15.1
5	770.13	670.23	663.31	644.72	642.24	642.56	643.78	645.21	
6	691.38	646.56	630.53	625.61	627.22	627.94	631.61	637.01	
7	667.29	609.03	604.01	603.21	608.58	612.30	617.81	625.16	
8	602.73	572.82	572.56	579.33	587.09	595.61	602.97	609.86	
9	511.31	526.41	536.19	563.21	567.01	578.91	589.61	597.60	
10	449.94	478.86	505.94	527.66	547.77	564.05	577.14	587.11	
11	428.96	441.47	476.97	505.23	531.51	551.34	566.26	578.52	
12	438.96	438.96	467.48	484.07	522.27	543.63	559.64	572.11	
13	438.24	438.24	476.93	516.91	541.41	562.83	578.39	589.88	
14	447.52	469.06	507.23	546.44	570.13	587.08	599.59	608.47	15.2
16	463.43	486.36	526.52	568.27	581.43	594.12	599.92	604.22	
16	476.88	518.57	563.38	573.37	581.87	599.58	600.16	599.29	
17	511.44	563.96	585.27	599.70	604.80	603.87	601.16	596.11	
18	527.65	573.99	596.58	600.88	597.88	592.36	586.12	575.39	
19	537.85	584.47	596.10	592.31	584.11	576.11	564.73	563.73	
20	564.11	608.48	608.73	597.79	584.84	571.36	566.48	546.82	
21	538.57	576.44	568.67	561.66	536.52	522.58	511.03	488.73	
22	533.76	560.67	540.41	518.00	500.88	487.56	477.23	467.81	
23	648.56	619.74	576.05	540.98	521.96	504.67	480.23	479.32	
24	746.96	651.73	603.21	566.21	526.27	506.98	489.62	477.67	
26	826.89	639.40	573.31	542.65	517.63	498.63	483.89	474.97	
27	876.82	580.81	542.22	516.30	484.46	476.41	465.40	469.60	
28	698.51	518.86	484.36	476.97	460.33	447.65	440.40	436.52	
28	484.30	466.68	431.03	421.84	412.13	399.92	396.98	394.47	
29	413.04	389.28	377.37	372.77	370.05	360.96	360.96	360.96	
30	382.88	368.02	366.24	366.24	366.24	366.24	366.24	366.24	15.3
31	374.62	371.52	371.52	371.52	371.52	371.52	371.52	371.52	
32	379.62	379.62	379.62	379.62	379.62	379.62	379.62	379.62	
33	371.52	371.52	371.52	371.52	371.52	371.52	371.52	371.52	
34	366.52	366.52	366.52	366.52	366.52	366.52	366.52	366.52	
35	387.52	387.52	387.52	387.52	387.52	387.52	387.52	387.52	
36	439.44	439.44	439.44	439.44	439.44	439.44	439.44	439.44	
37	439.44	439.44	441.58	473.29	507.44	576.12	602.79	784.91	
38	400.72	400.72	402.86	421.09	463.63	538.39	642.71	860.70	
39	369.92	369.92	369.92	369.92	411.42	436.41	505.16	617.54	
40	389.65	377.52	377.52	377.52	405.39	434.53	500.26	675.28	
41	408.28	388.11	388.11	378.00	407.27	436.30	488.87	714.88	
42	420.66	402.78	389.12	389.21	407.28	431.27	484.15	668.64	
43	387.13	380.06	369.63	369.63	374.78	389.12	432.82	569.08	
44	366.49	346.54	337.70	338.72	341.57	358.07	372.43	467.20	
46	396.00	386.67	379.89	379.71	389.08	388.62	411.42	461.46	15.34
46	466.86	446.98	431.71	426.89	428.76	436.54	461.14	536.70	
47	474.48	449.03	429.78	419.16	414.26	422.08	440.22	533.08	
48	469.57	434.88	414.71	401.43	393.07	395.56	416.10	463.98	
49	462.30	436.40	416.97	399.67	386.48	386.83	397.54	406.67	
50	472.66	447.16	426.07	406.21	388.82	382.70	384.34	377.61	
61	483.93	460.01	436.36	413.52	392.88	380.44	376.62	369.60	
62	444.85	475.55	447.38	422.56	397.92	379.79	371.23	369.60	
63	471.74	484.09	461.83	433.73	405.18	382.40	369.60	369.60	
64	607.88	609.23	477.16	446.72	416.38	386.48	371.75	369.60	
66	561.09	521.77	492.79	469.96	428.89	393.46	371.75	369.60	
67	544.79	532.94	510.46	478.01	444.59	407.55	369.99	369.60	
67	537.16	541.10	528.86	489.87	463.20	426.11	378.44	369.60	
68	533.69	647.09	646.46	636.96	608.43	447.76	369.64	369.60	
69	529.67	551.79	568.51	562.04	520.10	476.06	427.99	374.36	15.42
70	524.69	562.48	673.70	675.00	667.26	612.33	463.02	500.22	
71	513.94	568.36	586.34	597.12	597.16	578.66	512.26	631.72	
72	546.52	678.70	689.86	622.84	642.99	676.47	621.14	660.96	
73	582.06	674.06	609.08	648.14	699.56	730.98	722.28	676.70	
74	669.43	679.00	609.38	666.10	729.77	749.77	771.75	674.32	
75	636.03	676.07	609.67	646.06	729.76	746.34	824.47	692.43	
66	534.36	571.30	608.27	640.22	729.76	763.37	887.17	786.76	
67	548.87	573.73	608.54	666.84	729.76	752.91	883.14	925.12	
68	660.81	670.89	602.36	666.44	729.76	738.73	812.69	1248.22	
69	662.83	662.31	604.32	632.89	711.43	731.40	763.60	1210.694	
70	644.17	666.22	669.41	693.09	661.57	712.61	713.61	838.62	
71	640.46	661.36	663.48	677.21	604.21	653.86	666.68	669.01	15.46
72	638.57	660.36	661.60	674.77	690.63	606.68	610.94	692.41	
73	638.27	647.67	669.97	673.64	686.96	600.26	607.07	614.83	
74	639.21	646.01	669.66	671.29	691.01	699.44	621.36	633.13	

Fig.35 Mapping of stringer bay cross sectional areas for the optimum design

The average super stiffener section is 524 mm².

As shown in figure 35, the super stiffeners with the largest section area are situated in the fuselage bottom whereas the fuselage middle is characterised by the application of smaller super-stiffeners.

The section is larger in the bottom because bottom panels support larger stresses.

The high sections found in inter-frames 38-39, panels 15.1 and 15.3 are due to the stress concentrations around cargo door corners in the frame bay 37-38.

The high sections found in inter-frame 45-46, panels 15.3 and 15.46 are due to the stress concentrations around centre wing box corners in the frame bay 46-47.

The section is small around the minimum design zone which supports less stresses than others panels, only a low shear stress (see red cells on the Fig.35 with section for each super stiffener).

Bitener Number	Frame 32-38 Frame 38-40 Frame 40-41 Frame 41-42 Frame 42-43 Frame 43-44 Frame 44-46 Frame 46-48								Panel
	116	117	118	119	120	121	122	123	
2	2.66	2.68	2.64	2.62	2.61	2.60	2.59	2.59	
3	2.90	2.83	2.62	2.59	2.58	2.57	2.57	2.56	
4	2.94	2.83	2.58	2.56	2.54	2.54	2.54	2.54	16.1
5	2.71	2.57	2.53	2.50	2.50	2.50	2.50	2.51	
6	2.54	2.49	2.45	2.44	2.44	2.44	2.45	2.47	
7	2.53	2.37	2.36	2.36	2.37	2.40	2.42	2.43	
8	2.31	2.24	2.24	2.27	2.30	2.34	2.36	2.38	
9	1.99	2.07	2.11	2.17	2.22	2.27	2.31	2.34	
10	1.71	1.85	1.97	2.07	2.15	2.21	2.26	2.30	
11	1.60	1.67	1.84	1.98	2.08	2.16	2.22	2.27	
12	1.60	1.60	1.75	1.92	2.04	2.13	2.19	2.24	
13	1.60	1.60	1.79	1.96	2.07	2.16	2.22	2.26	
14	1.60	1.66	1.89	2.05	2.14	2.21	2.26	2.29	16.2
15	1.63	1.79	1.98	2.10	2.19	2.23	2.26	2.27	
16	1.74	1.95	2.09	2.18	2.23	2.26	2.26	2.26	
17	1.92	2.11	2.21	2.26	2.27	2.27	2.26	2.23	
18	2.05	2.24	2.30	2.31	2.30	2.27	2.25	2.21	
19	2.15	2.33	2.36	2.34	2.30	2.27	2.22	2.18	
20	2.27	2.43	2.42	2.37	2.32	2.26	2.21	2.16	
21	2.31	2.44	2.41	2.33	2.27	2.21	2.16	2.10	
22	2.32	2.41	2.33	2.24	2.17	2.11	2.06	2.02	
23	2.45	2.50	2.36	2.25	2.16	2.08	2.02	1.97	
24	2.72	2.60	2.40	2.28	2.17	2.09	2.02	1.96	
25	3.16	2.96	2.36	2.25	2.15	2.07	2.00	1.96	
26	3.62	2.40	2.26	2.16	2.07	2.00	1.94	1.91	
27	2.55	2.19	2.02	2.00	1.93	1.89	1.84	1.82	
28	2.12	2.00	1.90	1.83	1.79	1.71	1.69	1.68	
29	1.89	1.76	1.71	1.68	1.66	1.60	1.60	1.60	
30	1.68	1.60	1.60	1.60	1.60	1.60	1.60	1.60	16.3
31	1.60	1.60	1.60	1.60	1.60	1.60	1.60	1.60	
32	1.60	1.60	1.60	1.60	1.60	1.60	1.60	1.60	
33	1.60	1.60	1.60	1.60	1.60	1.60	1.60	1.60	
34	1.60	1.60	1.60	1.60	1.60	1.60	1.60	1.60	
35	1.60	1.60	1.60	1.60	1.64	1.72	1.77	1.80	
36	1.60	1.60	1.60	1.67	1.81	1.96	2.43	3.00	
37	1.60	1.60	1.61	1.77	1.94	2.25	2.79	3.44	
38	1.60	1.60	1.61	1.70	1.97	2.32	2.84	3.44	
39	1.60	1.60	1.60	1.60	1.67	2.07	2.31	2.75	
40	1.67	1.60	1.60	1.60	1.77	1.96	2.21	2.63	
41	1.79	1.66	1.66	1.60	1.78	1.95	2.30	2.98	
42	1.87	1.76	1.66	1.67	1.78	1.92	2.14	2.71	
43	1.88	1.76	1.60	1.67	1.69	1.88	2.03	2.45	
44	1.73	1.67	1.60	1.60	1.60	1.73	1.78	2.18	
45	1.78	1.74	1.70	1.70	1.72	1.73	1.82	2.08	16.34
46	2.04	1.94	1.86	1.83	1.84	1.88	2.00	2.33	
47	2.11	2.00	1.90	1.84	1.81	1.85	1.95	2.34	
48	2.00	1.97	1.86	1.79	1.74	1.75	1.86	2.07	
49	2.08	1.97	1.86	1.78	1.70	1.70	1.76	1.81	
50	2.12	2.02	1.90	1.81	1.71	1.68	1.69	1.66	
51	2.17	2.07	1.96	1.85	1.73	1.67	1.64	1.60	
52	1.99	2.11	2.00	1.89	1.76	1.67	1.61	1.60	
53	2.03	2.16	2.05	1.94	1.80	1.68	1.60	1.60	
54	2.29	2.20	2.11	1.99	1.85	1.70	1.61	1.60	
55	2.25	2.23	2.15	2.05	1.92	1.74	1.61	1.60	
56	2.27	2.25	2.20	2.11	1.99	1.81	1.60	1.60	
57	2.27	2.27	2.25	2.17	2.06	1.90	1.65	1.60	
58	2.26	2.25	2.25	2.24	2.14	2.00	1.77	1.60	
59	2.25	2.30	2.32	2.30	2.23	2.10	1.91	1.63	16.42
60	2.24	2.31	2.35	2.35	2.31	2.20	2.05	2.02	
61	2.23	2.35	2.37	2.40	2.39	2.34	2.19	2.44	
62	2.34	2.39	2.39	2.45	2.56	2.75	2.88	2.57	
63	2.42	2.38	2.42	2.55	2.88	3.03	3.03	2.74	
64	2.34	2.38	2.43	2.59	3.08	3.21	3.35	2.72	
65	2.25	2.38	2.43	2.53	3.08	3.31	3.69	2.83	
66	2.30	2.39	2.45	2.50	3.08	3.30	4.10	3.44	
67	2.36	2.40	2.47	2.60	3.08	3.23	4.07	4.35	
68	2.39	2.41	2.47	2.59	3.08	3.14	3.61	5.44	
69	2.37	2.40	2.44	2.55	2.96	3.09	3.39	6.24	
70	2.35	2.38	2.42	2.46	2.67	2.97	2.96	3.78	
71	2.35	2.38	2.41	2.44	2.48	2.69	2.68	2.76	16.48
72	2.35	2.38	2.41	2.44	2.46	2.52	2.54	2.47	
73	2.35	2.38	2.41	2.44	2.47	2.51	2.51	2.52	
74	2.35	2.37	2.41	2.44	2.48	2.51	2.51	2.54	

Fig.36 Mapping of pocket thicknesses for the optimum design

The average skin thickness is 2.17 mm.

The thickness mapping is fully in agreement with the super-stiffener section area mapping as shown on Fig.36. The same interpretations applies to the section areas.

VI. Loose coupling ¹⁶

To reach the level of a full fuselage cover optimisation, the tight coupling approach can be very greedy in terms of processors. To achieve the same computational times as for a barrel, the hardware need is about ten times higher, i.e., 300 processors. Such a large number of processor is not necessary available even in a large company.

This is the reason why another approach, named loose coupling was explored.

This approach consists in replacing the call to stress analysis tools (here ASSIST) by a call to a surrogate model. More information on surrogate modelling is provided in the chapter

dedicated to optimisation. More references can also be found in [17,18]. Note that surrogate modelling is also referred to as meta-model or response surface.

A. Surrogate models for stress tools

Initially the intent was to approximate stress responses, that is to say to replace stress tools with surrogate models but two drawbacks had to be considered:

- the optimisation is still to be made. Even if the surrogate models are quicker than ASSIST there is a large number of optimisations to be done and it takes time.
- the number of inputs is quite large to build a surrogate model.

Indeed with the local optimisation problem exposed in section 3, the inputs of the surrogate model are:

- stringer height
- web stringer thickness
- free flange width
- free flange thickness
- attached flanged thickness
- skin thickness
- F_{XSR}
- N_{xy}
- Pitch
- Curvature radius

Note that the loading has been simplified and that the sizing process (considering that the main sizing criteria for the barrel was buckling) has been reduced to buckling/post-buckling only. The total number of inputs is then 10 as listed above. To cover such a design space, a very large number of samples is needed, which in turn, requires a very large number of computations. This is the well-known problem of “curse of dimensionality”.

Nevertheless the attempt was made and a specific piecewise approach was used to consider the non-linear responses of ASSIST. This piecewise approach consists in mixing various Neural Networks and is called MoE (Mixture of Experts). Neural Networks are well known to cover highly non-linear responses with a capability to generalisation and extrapolation.^{19,20} The MoE approach gives a pragmatic answer to the curse of dimensionality.^{21,22}

However it took a long time to understand the non-linearity of the software and to put in place the appropriate MoE. For this reason, this approach was not considered mature enough for industrial application: additional research work is still needed.

B. Design curves

The alternative approach was to directly approximate the optimisation results. The advantage in doing so is that all optimisation design variables disappear from the input space. Moreover the optimisation is done a priori and is not to be done inside the global loops: the surrogate models have just to be calculated with appropriate internal loads to get the minimum thickness and minimum section area. If there are multiple load cases, the most conservative values for skin thickness and stringer section area are selected.

The resulting set of inputs to be considered is:

- F_{XSR}
- N_{xy}
- Pitch
- Curvature radius

The outputs are restricted to the minimum thickness and the minimum area found with the local optimisation.

In this case, because of the reduced dimension of the input space, the computational effort becomes much more reasonable and a surrogate model approach can really be considered for the approximation. Moreover as aforementioned, with this approach, the local optimisation is no longer necessary at global level. It is replaced by a simple interrogation of the design curve. It is then much more computational efficient as shown in section 6.3.

This design curve gives for each set (F_{XSR} , N_{XY} , p , R) the minimum skin thickness and the minimum stringer area as resulting from the local optimisations.

On top of that, the detailed design variables can also be derived and the stinger profiles designed.

Again some preliminary studies show that Neural Net (NN) was the surrogate model the most appropriate to the non-linear responses to be approximated. More information on neural networks is provided in the optimisation chapter or in [19,20].

In the first attempt described in paragraph 1 (analysis regression), the dimension of the input space had required to use filling space DoEs like Latin Hyper Cube. In this new approach, the significant reduction of the input dimension (from 10 to 4) authorizes the use of a full factorial DoE.^{23,24}

For the training of the NN, a specific BOSS Quattro session was then used as shown on Fig.37: it is a double parametric session. The parametric task implements the factorial DoE and drives an optimisation task: The optimisation is to be run for all quadruplets of the DoE as illustrated on Fig.38.

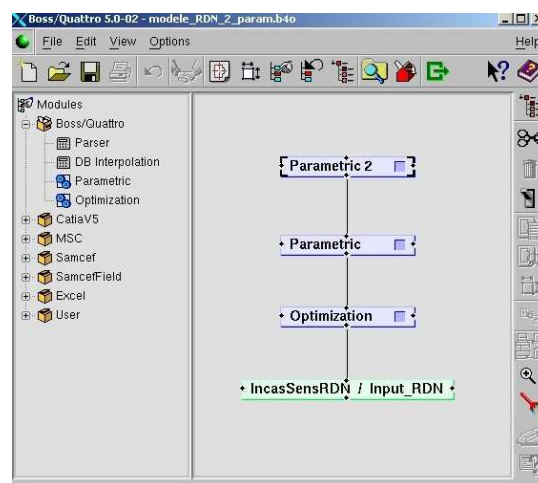


Fig.37: Main GUI window for neural net

Since (pitch, radius curvature) couples are discrete values, a double parametric session is used:

- parametric 1 for continuous inputs : compression and shear combination
- parametric 2 for discrete inputs: {pitch/radius curvature} couples

Upon running of the optimisation cases, results are extracted from output files *.log and are implemented in the training set.

Compression (Newtons)	10 000	25 000	50 000	75 000	100 000
	125 000	150 000	175 000	200 000	225 000
	250 000	275 000			

Shear (MPa)	5	30	50	70	90
	110	130			

Pitch / radius curvature (mm)	191.1/3300	202.7/3300	154.0/3430	132.4/5220	145.2/5220
	149.2/5220	154.0/5220	158.6/5220	165.2/5220	172.1/5220
	180.4/5220	191.1/5220	197.7/5220		

Fig.38: Full factorial DoE for the training set

The training will then be based on a training set with 1092 input cases (12x7x13).
7 outputs are extracted from *.log files:

- Web height
- Web thickness
- Attached flange width
- Attached flange thickness
- Free flange width
- Free flange thickness
- Skin thickness

7644 output cases (1092x7) will be used to build the neural network.

Neural network was built with the help of [19,20] following specifications:

- 1 hidden layer and sigmoidal activation
- Linear output Layer

Remark: sigmoidal activation refers to the transfer function of each neuron (regularisation of a heaviside function).

The MATLAB Neural Network toolbox was used to build the neural net.²⁵ Four nets were performed:

- with 40 neurons
- with 50 neurons
- with 60 neurons
- with 70 neurons

The convergence of the training process is illustrated in Fig.39.

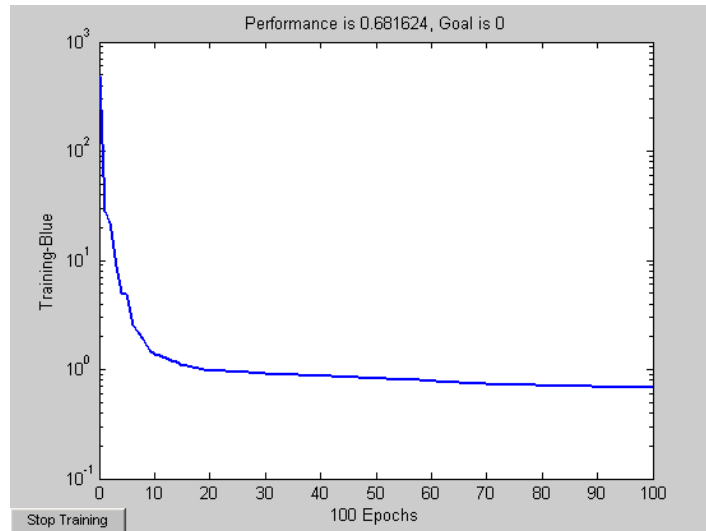


Fig.39: Mean Square Error (MSE) for 40 neurons

Quality of the neural network can be checked using 3 methods:

- Mean Square Error (MSE) value
- Comparison between training set output and neural net output
- Comparison between neural net output and BOSS QUATTRO session using the same inputs (Test base)

More information on the quality of surrogate model fits can be found in the optimisation chapter.

Comparison is made on super stiffener section area that is computed using each output as shown on Fig.40.

	40 neurons	50 neurons	60 neurons	70 neurons
MSE	0.68	0.43	0.36	0.35
Difference training set/neural net output				
- min/max	-23/ 16.7	-12.4 / 14.6	-14.1 / 9.1	-12.2 / 16.1
- relative mean error	-0.02	-0.05	-0.038	-0.042
- absolute mean error	2.44	2.09	1.67	1.72
Difference neural net output /test base				
- min/max	-6.5 / 6.9	-4.4 / 5.9	-3.7 / 8.0	-2.4 / 4.0
- relative mean error	-0.16	-0.32	0.028	0.028
- absolute mean error	2.15	1.94	1.74	1.26

Fig.40: Training results

The accuracy target which was pursued was a min/max error of less than 5%. However it was not possible to drive directly this error measure and find automatically the optimum number of neurons. This is the reason why the several NNs were built for 40, 50, 60 and 70 neurons.

Fig.41 shows that a 70 neurons neural net seems to give a satisfactory accuracy (min and max value under 4% with test base comparison).

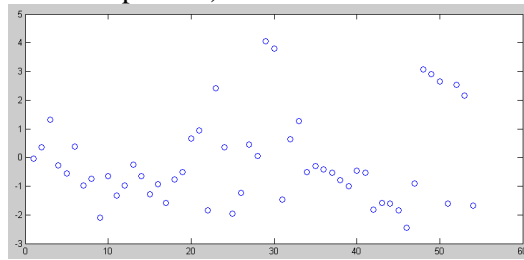


Fig.41: Training set target and test base error with 70 neurons

The following figures 42 show response surfaces of super stiffener section area for target (left) and 70 neurons neural net (right).

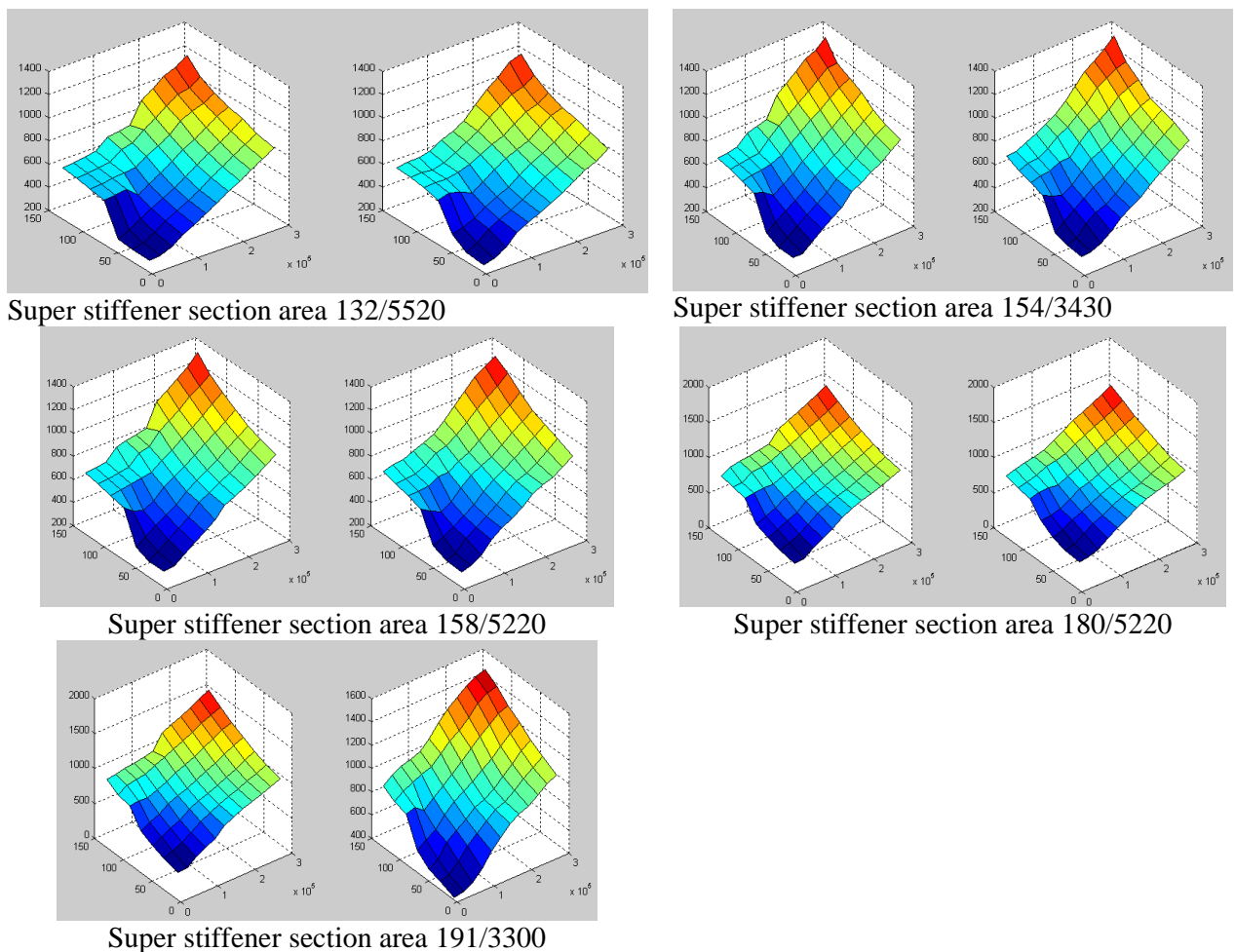


Fig.42: Response Surface for section area found for various (pitch, curvature radius) couples

C. Demonstration

A demonstration was then made on the full barrel test-case.

For that a new version of STIFFOPT was developed based on this loose coupling approach.

It just consists in replacing calls to BOSS Quattro by a call to the design curves. The sizing is then performed internally to PATRAN based on a PATRAN Command Language (PCL). The optimisation speed is then becoming very fast.

A new window (Fig.43) has been added in GUI STIFFOPT. The user can choose “neural net” method when he defines optimisation method.

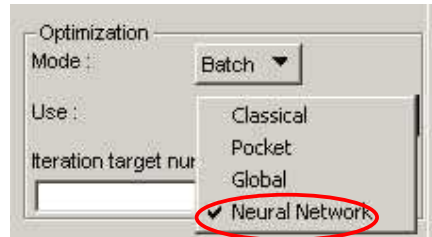


Fig.43: STIFFOPT optimisation window

This new approach is, of course, very competitive with respect to the tight coupling one. However it is worth mentioning that the accuracy will always be questionable. This is the reason why this approach is not recommended for detailed design when the utmost weight savings are sought for the structure.

1. Tight coupling convergence

Figure 44 depicts the results of the 3 optimisation loops were performed with tight coupling. The 1st optimisation is made with initial values identical to neural net session initial values. Optimisation 2 and 3 are computed with optimized results values (respectively optimisation 1 results and optimisation 2 results).

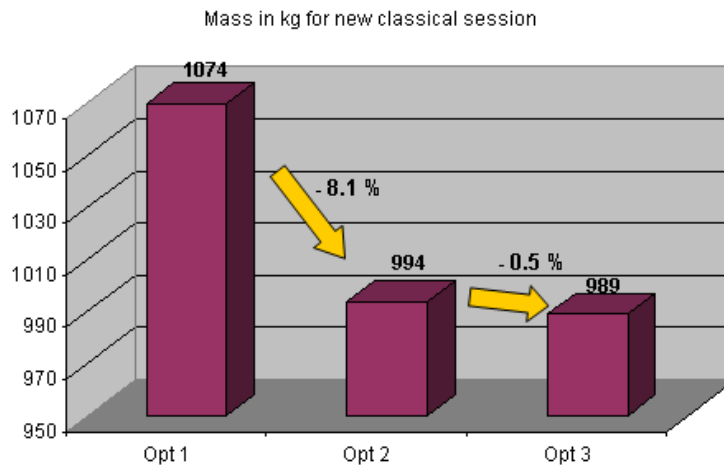


Fig.44: Mass decrease for 3 optimisation loops

Mass decreases by 8.1 % after the first optimisation, then decreases again by 0.5 %. Convergence is reached after the 3rd optimisation loop. This first optimisation is performed with high initial values which do not lead to an optimum. The 2nd optimisation is made with values already optimized and the optimum is consequently lower.

2. Convergence with neural net optimisation

Seven optimisations loops are performed using multi-init neural net. As it can be seen from Fig. 45, convergence is reached as soon as the 2nd optimisation. Mass decreases or increases slightly within 0.1 % after the 2nd optimisation.

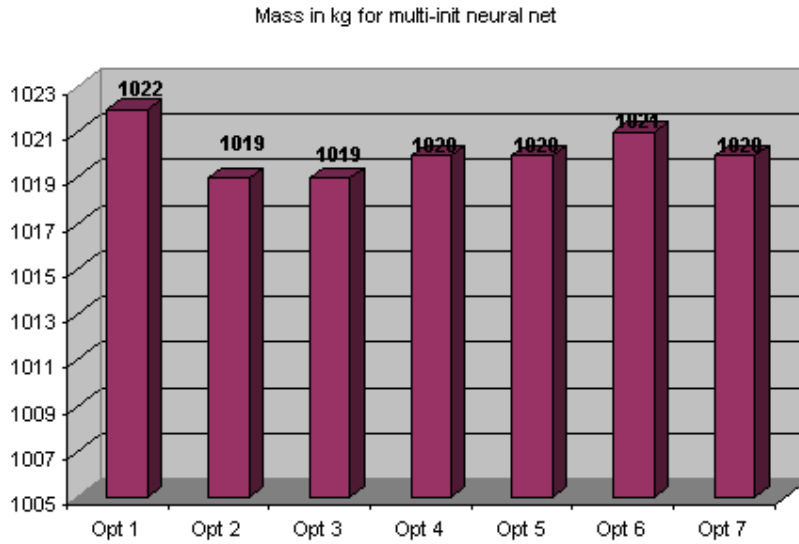
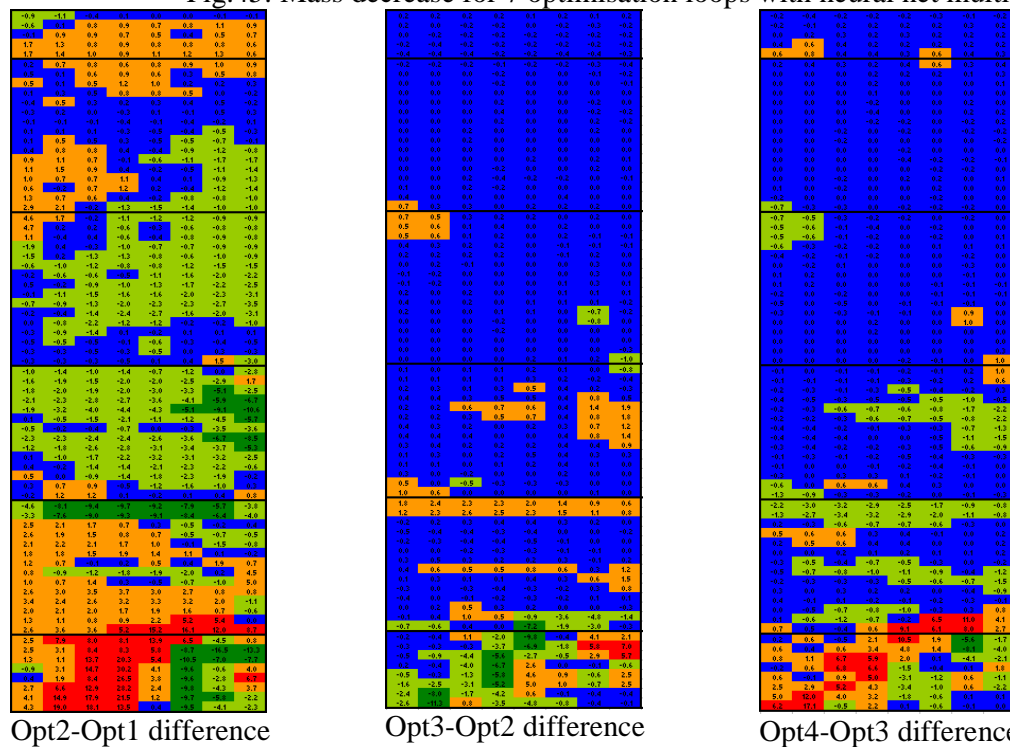


Fig.45: Mass decrease for 7 optimisation loops with neural net multi-init



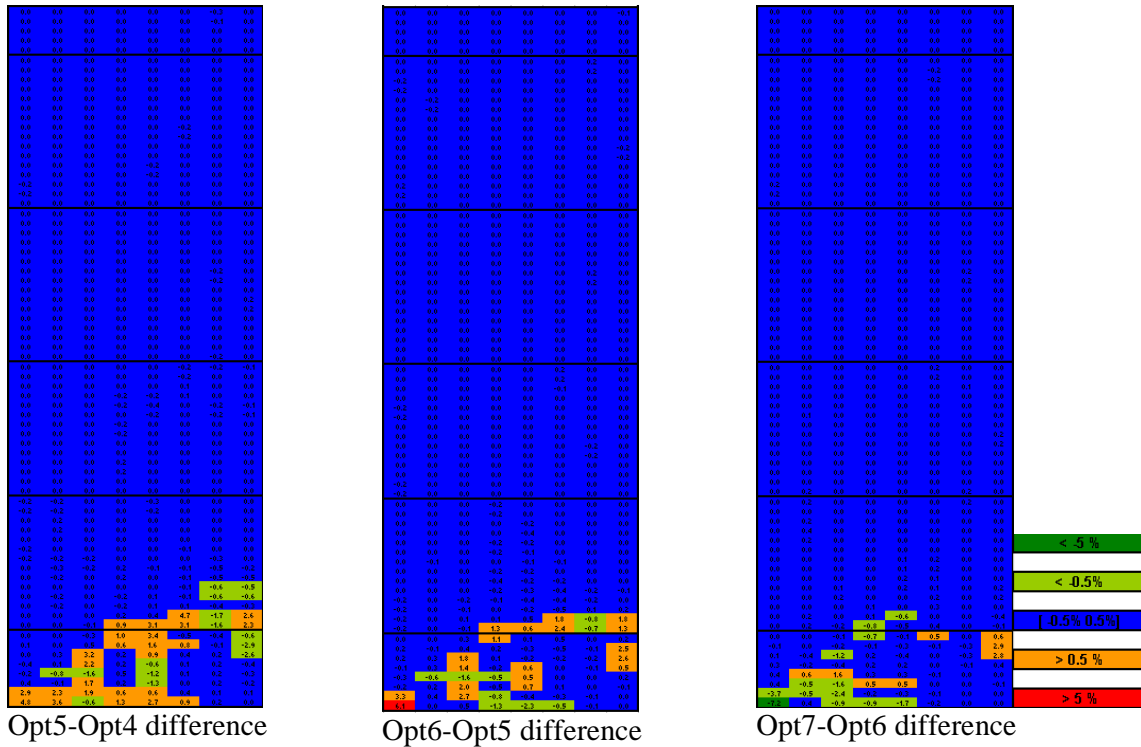


Fig.46: Section difference for each super stiffener between 2 optimisation loops

Even if global mass is stabilized after the 2nd optimisation loop, figure 46 shows there is a slight redistribution of internal loads and super-stiffener section areas along subsequent iterations.

3. Comparison classical and neural net optimisation

Mass in kg	New classical session	Multi-init neural net	Delta (%)
Optimisation 1	1074	1022	-4.2
Optimisation 2	993.6	1019	2.4
Optimisation 3	988.7	1019	2.9

Fig.47 Comparison between tight and loose coupling

After three optimisation loops, a difference of about 30 kg still exists between new classical results and neural net results (see Fig.47).

Despite multi-init use allowing to avoid local minima, an optimisation with a neural net is limited by initial values: the convergence of local optimisations is probably better due to the fact that the same optimisation is reconsidered several times along upper iterations with close starting points. This enforces the convergence.

Another reason is also an insufficient accuracy of the neural net, which was found to be around 4% (see Figure 40).

VII. Additional considerations

Other developments have been made to refine and complete the STIFFOPT optimisation process.

A specific option has been implemented to focus the optimisation on skin pockets each time this pockets are sized by a buckling on-set criterion. This is complemented by a stringer only optimisation, which can be run subsequently to complete the detailed sizing.

Another option has also been added to smooth the design after optimisation. Because the optimisation is local, it is necessary at the end to harmonise the stringer dimensions, for example, in order to have a constant stringer height.

Finally a comparison was made between the STIFFOPT optimisation process and a more complete one with an optimum control of the internal load redistribution. This was implemented by including the neural net equations as constraints inside the optimisation module of NASTRAN: SOL200. The comparisons made show that both sizing optimisation approaches give similar results. However caution needs to be exercised: this result does not mean that the optimisation processes are equivalent, but only that in case of the considered test-case, they are comparable. It is well known that there is no equivalence, particularly when some stiffness criteria drive the design.

VIII. Refinement of local optimisation^{26,27}

As mentioned before the tight coupling optimisation is particularly recommended for detailed design while the surrogate model approach is probably the most suited for rapid sizing optimisation both for reason of computational times and accuracy.

However, considering that detailed design is usually trying to find the lightest structure possible within a giving margin policy, the question of whether to use higher fidelity methods rather than analytical engineer-based ones can be asked.

Indeed numerical simulation of stability is becoming more and more common practice and the trend is now to replace tests with such numerical simulation approaches (virtual testing). The next step will probably be to perform optimisation based on virtual testing. There are few references in the literature to address this kind of topics and the complement of tests is often necessary to the optimisation process.²⁸

This is the goal of this section to present such an approach developed inside SAMCEF MECANO and demonstrated at panel level.²⁹

The idea behind is simply to replace the ASSIST analysis by the SAMCEF MECANO finite element based simulation, in order to have the STIFFOPT framework based on virtual testing approaches.

A. The panel use-case

It is worth mentioning first the targeted application. The fuselage barrel is considered to be split into local finite element models to analyse the stability. The buckling/post-buckling behaviour is considered local which means that an instability can only occur within a frame bay. In fact the local finite element model is a kind of numerically based ASSIST.

Due to the current trends followed by the civil aeronautical industry, including this project, it was also decided to focus on composite materials.

The panel use-case used here is a panel representative of the behaviour of a Carbon Fiber Reinforced Plastic (CFRP) fuselage with seven omega stringers (Fig.48). Boundary conditions are simplified for demonstration to single supported sides.

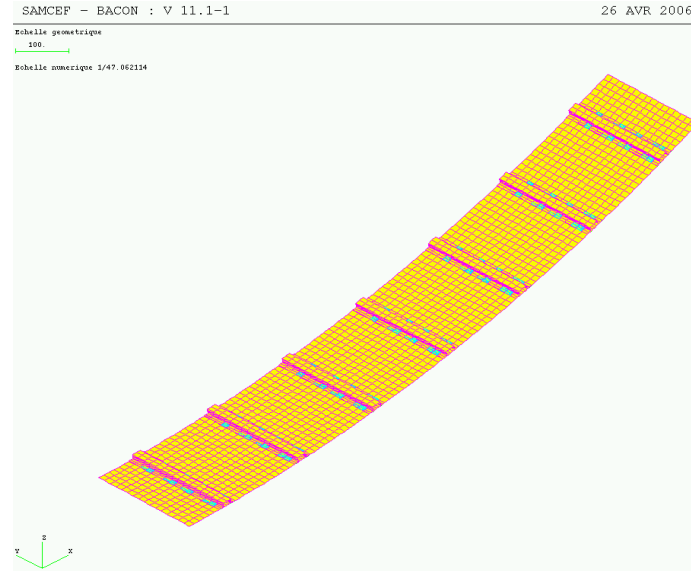


Fig.48 the panel use-case

The corresponding finite element model was built with SAMCEF. Note that this model has 17326 nodes, 16000 cells and 109777 degrees of freedom.

The definition of the optimisation problem was intentionally simplified to focus the demonstration on the integration of non-linear analysis in a gradient-based optimisation tool.

The angle are considered as fixed to standard orientations: $0^\circ, -45^\circ, 45^\circ, 90^\circ$. The difficulty to address angle variables directly has been demonstrated in [30].

The stacking sequence itself is not considered as designable, even if we have developed at AIRBUS a simplified optimisation process linking the stacking sequence to the thickness and producing manufacturable covers.^{31,32}

We finally based here on a homogenized representation of the composite lay-up using only angle thicknesses as design variables.

Design variables are ply thicknesses for each ply orientation ($0^\circ, 45^\circ$ and 90°), for each one of the seven super-stringers. A distinction is made between thicknesses for skin panels and for stringers. This amounts to considering $3 \times 7 \times 2 = 42$ design variables. In the sequel, we denote them as follows:

- for the skin panels: $t_{angle}^{SKIN,i}$, with $i \in \{1, \dots, 7\}$ and $angle = 0^\circ, 45^\circ$ or 90° ;
- for the stringers: $t_{angle}^{STRINGER,i}$, with $i \in \{1, \dots, 7\}$ and $angle = 0^\circ, 45^\circ$ or 90° .

Lower and upper bounds on these variables are set to 0.4 and 2 mm respectively.

The objective function is the weight – to be minimized.

Constraints are expressed as follows:

1. *buckling reserve factor*: $RF_{buckling} \geq 0.76$
2. *collapse reserve factor*: $RF_{collapse} \geq 1$.

The objective function, the buckling RF and their sensitivities are computed by a linear finite element analysis while the collapse reserve factor and its sensitivity are provided by a nonlinear analysis.

B. Development of sensitivities for Non Linear Finite Elements Analysis (NLFEA)

The nonlinear analysis is performed by SAMCEF Mecano, a finite element software package which solves nonlinear structural and mechanical problems.

The general framework of the research work and results we describe here is solving the optimization problem defined in Section 2, where one of the constraints takes the form:

$$RF_{collapse} \geq 1.$$

Our objective was twofold:

- find a suitable way to compute this result on the basis of results provided by the nonlinear analysis;
- ensure that the sensitivities of this result (with respect to all design variables) may be computed.

An obvious choice for the collapse RF is the load factor, which we denote by λ in the sequel. As an illustration, let us consider a simple super stiffener subject to both compression and shear loads. Assume that loads are applied progressively, the full loads (100%) corresponding to time 1. The nonlinear analysis terminates at time $t \approx 0.566$ (that is largely before the full loads are applied) because time steps become too small. This means that for the given value of the design variables only 56.6% of the loads can be applied before collapse occurs.

In this case we could thus have taken

$$RF_{collapse} = \lambda = t \approx 0.566.$$

Figure 49 below shows the displacement of a node (belonging to the skin panel of the super-stiffener) along the z-axis.

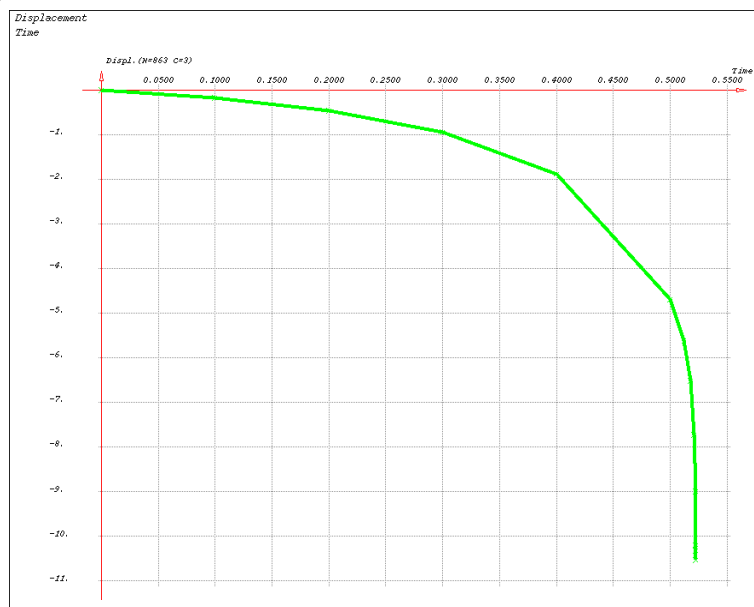


Fig.49 Load versus displacement diagram for the non-linear analysis

However this way to compute the collapse RF is not fully satisfactory since the sensitivity of λ is not directly available from a nonlinear analysis. This is why we have chosen to derive such a sensitivity using another method for the nonlinear analysis, namely Riks continuation method.³³ While classical Newton methods could have problems when passing a limit-point (because the generalized load displacement curve may have a decreasing time along the curve), continuation methods (also called *arc-length* or *Riks* methods) involve an additional parameter, namely the arc-length (denoted by s in the sequel), which is controlled in place of the time.

Due to this additional variable being introduced, an additional equation is added to the system of equations to describe the relation between the generalized displacements q and load λ on the one hand and the arc-length s on the other. The simplest form of this constraint equation, corresponding to a hyperplane perpendicular to the predictor, was first introduced by Riks..

In a similar way, we added one equation allowing computing the sensitivity,

$$\frac{\partial \lambda}{\partial a}.$$

We also constrained the unknown vector to be orthogonal to the load-displacement curve rather than a simple measure based on the vertical gap $\Delta\lambda$, which allows a better accuracy of the sensitivity measure as shown on Fig.50.

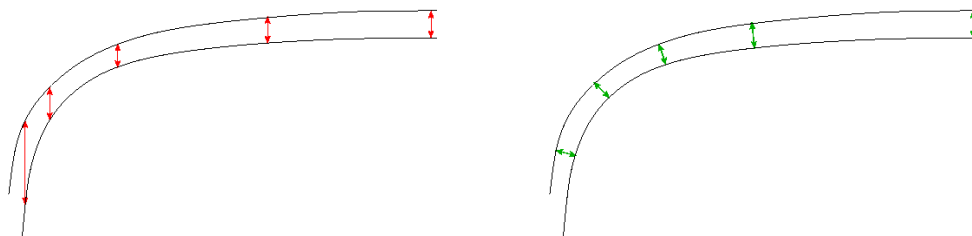


Figure 50 Sensitivity analysis with Riks method

Altogether, this methodology allowed us to derive a suitable algorithmic process for computing the value of the reserve factor and its sensitivity. This process was successfully implemented within a COTS tool (SAMCEF Mecano) and tested on a variety of examples. (Maybe it is possible to add a reference for this)

C. Panel optimisation

In this paragraph we show how the industrial application described in paragraph 8.1 can be solved in practice. We first briefly describe the problem formulation in the framework of an application manager before showing the results we obtained. To have a step by step approach buckling constraints only were considered in a first time.

1. Optimisation session

A complete computational process has been created, involving as many external tasks as the number of analyses, the latter being connected to the optimisation task, as illustrated on the screenshot in figure 51 below.

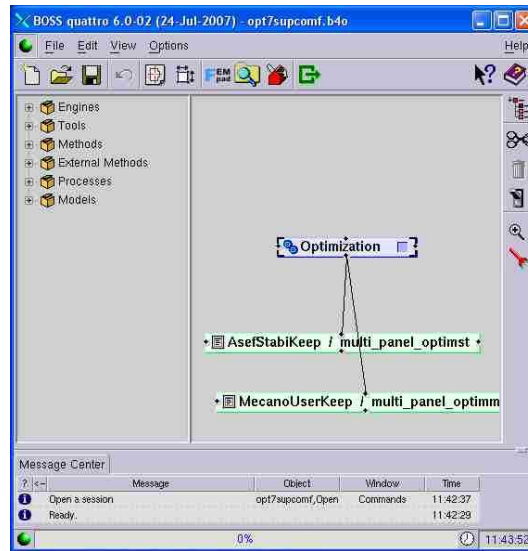


Figure 51 Main window with task tree of the optimisation process

Two different kinds of analyses are used:

- linear buckling analysis based on SAMCEF-Asef stabi to capture the buckling on-set for skin
- Non-linear finite element analysis to capture the panel collapse

Of course, any branch of the task tree can be removed in order to concentrate the optimisation on one criterion.

2. Linear buckling

In this section, we first focus on the solution of the linear buckling optimization problem, removing the collapse constraint from the above formulation. This would allow to bring in light a possible cause of erratic convergence, which is shown to come from an incomplete formulation of the optimization problem.

From a practical point of view, the buckling reserve factor is computed with SAMCEF Stabi, which is dedicated to the computation of buckling modes and related numerical results.

By definition, the first buckling load is of interest when designing a structure to withstand instability and this single value corresponds to the $RF_{buckling}$ constraint. However, due to mode-switching, there is no guarantee that the first buckling load always corresponds to the same buckling mode and as a consequence the related sensitivities are not necessarily relevant to the subsequent steps and may cause erratic convergence. This is the reason why, instead of using mode-tracking techniques, a small set of say n buckling loads is often actually computed, the $RF_{buckling}$ constraint being then a vector-valued result. Since all these n constraints must now be satisfied, mode-switching inside those n values is not an issue anymore.

Our initial tests were performed with $n = 12$ and they allowed us to see that, for some designs, the first buckling modes may not be representative of the overall structure. Indeed, it turns out that, at a given iteration, the buckling modes may only influence a small part of the structure, which will be designed, while the remaining structural parts are not sensitive. The panel thickness in the sensitive part could increase to satisfy the stability criteria, while the

thickness in the insensitive part will certainly reach its lower bound, since it is to be minimized. At the next iteration, the low-thickness part is likely to become sensitive to buckling because of a small local stiffness, while the remaining part could become insensitive to the restrictions. If repeated, this scenario leads to oscillations and deteriorates the convergence of the optimization process, as illustrated in figure 52.

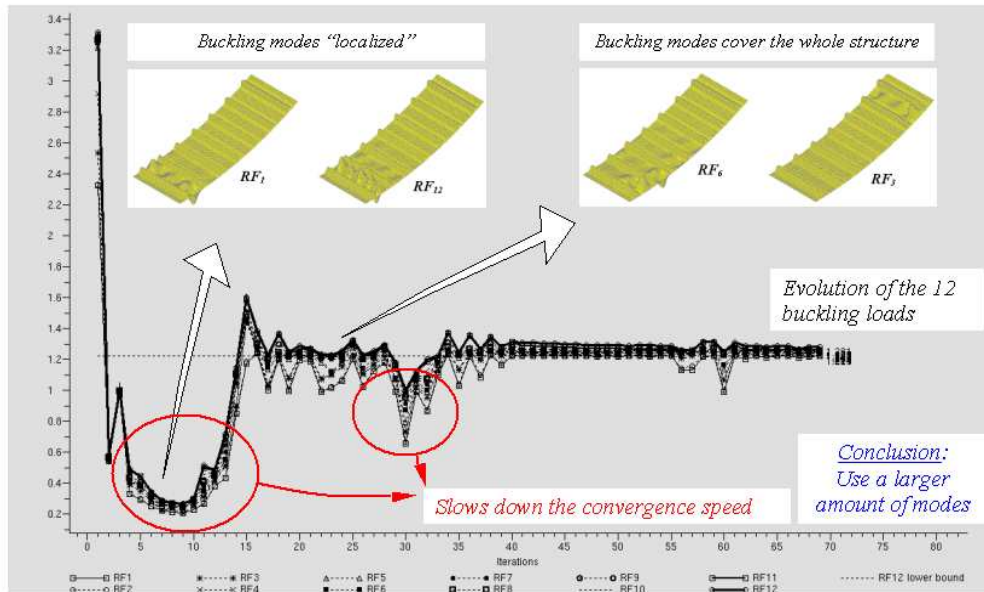


Figure 52 Optimisation convergence history for buckling reserve factors (initial)

When simple panels of limited size including few stiffeners are studied, or when the thickness design variables are defined over wide regions, local buckling modes are less likely to appear. Should this occur, they would anyway be supported by a design variable that covers a wide structural part. It turns that the values of the design variables are not only driven by a target on a minimum weight, but also by buckling considerations. When larger structures are studied, some design variables can become blind to the first (local) buckling modes used in the optimization problem. In such a case, the convergence difficulty discussed above is likely to happen.

Following this, we increased the value of n and set $n = 100$. The results obtained in this case were much better in the sense that only six iterations of the optimization process were required for convergence, as shown in figure 53.

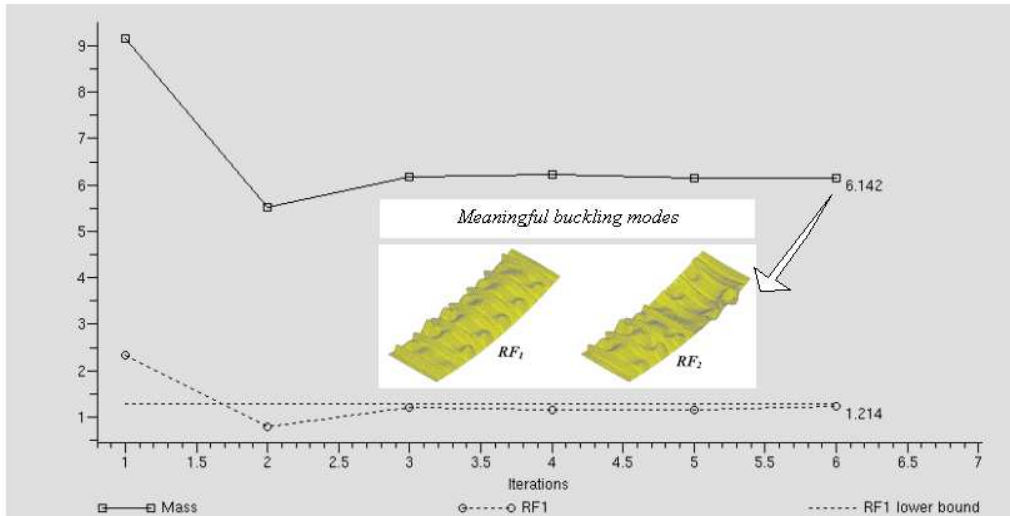


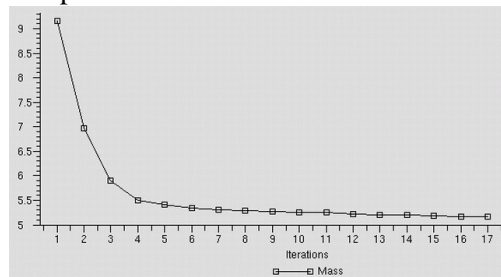
Figure 53 Optimisation convergence history for buckling reserve factors (improved)

This shows that a wide range of the first buckling loads must be used in the practical formulation of a linear buckling optimization problem. As was further illustrated by [34], using those larger sets not only makes the whole structure sensitive to buckling, but it also allows avoiding oscillations and/or slow convergence of the optimization process.

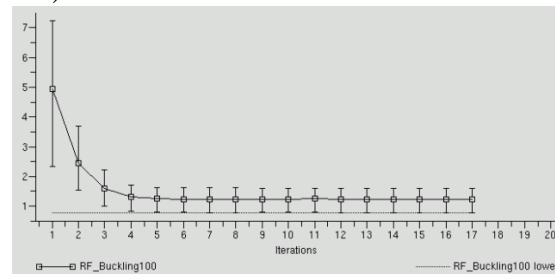
3. Non-linear finite element analysis

The optimisation run converged properly in 17 iterations. The curves displayed in Fig. 53 show the evolution of all three functions defining the optimization process; values displayed are those at optimum. Note that a tolerance on constraint violation (set to 2.5%) was used in accordance with AIRBUS practices. All constraints are thus satisfied at optimum.

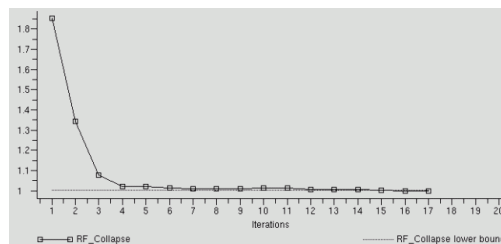
Also recall that the buckling reserve factor is computed as a vector-valued function with 100 values by SAMCEF (please put SAMCEF Stabi in reference) (hence the bars displayed in figure 54 represent these successive sets of 100 values).



Weight = 5.1513



$RF_{\text{buckling}} = 0.7531$



$RF_{\text{collapse}} = 0.9951$

Figure 54 Convergence history for the various responses

Both runs yield significant weight savings while reserve factors do not perturb the convergence of the process. The sequences of images in figure 55 show the evolution of structure response over a few iterations. The images on the left show displacements corresponding to the first buckling load while the images on the right show displacements at collapse.

Second run (margin policy: 0.76)

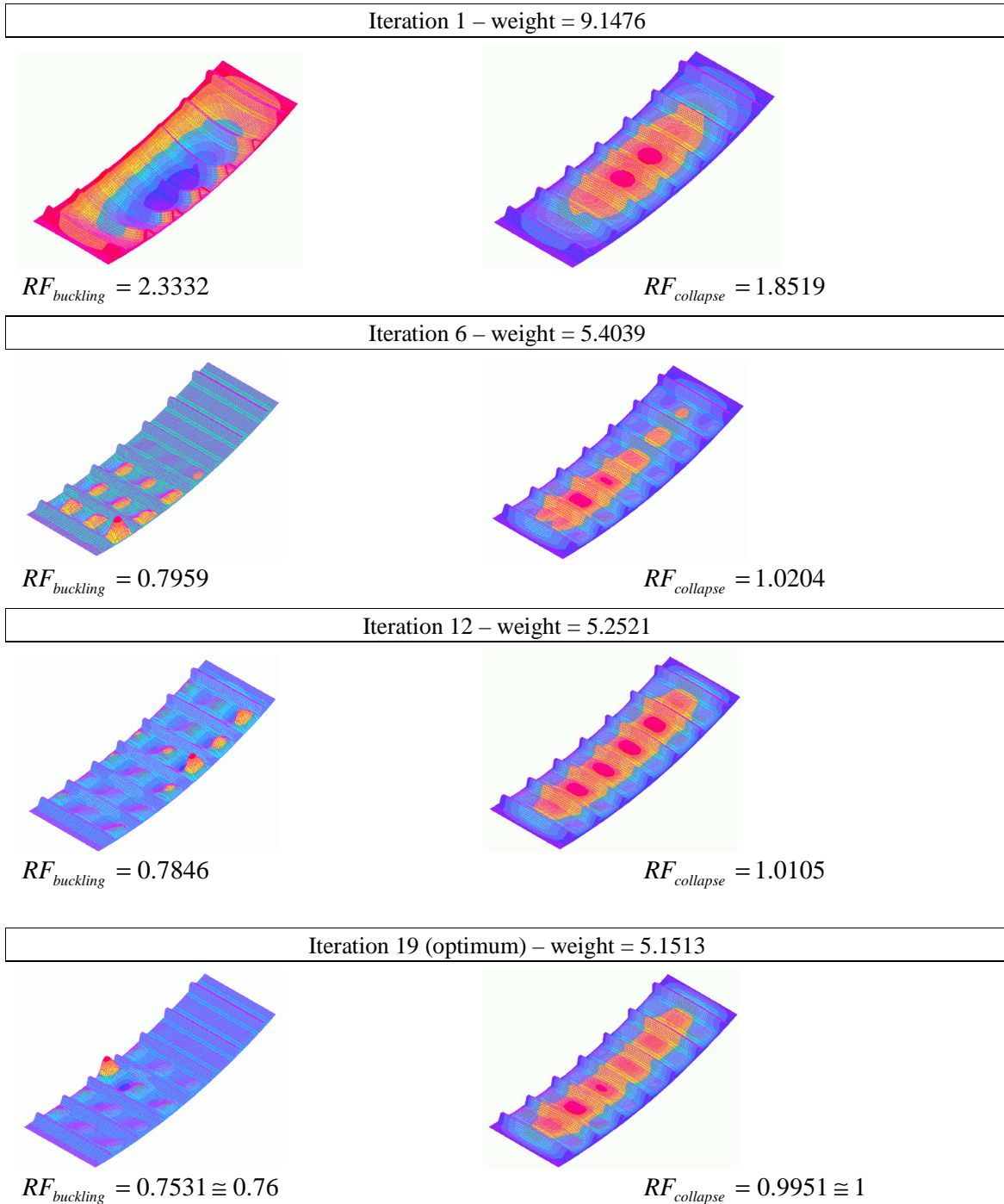


Figure 55 Buckling on-set and collapse modes for various iterations

The figure 56 shows the final values of the 42 design variables for both margin policies.

Number	Variable name	Value for margin 0.76
0	_R1_HOMSTY_3_1	0,4
1	_R1_HOMSTY_3_2	0,4
2	_R1_HOMSTY_3_4	0,4
3	_R1_HOM1_3_1	0,4
4	_R1_HOM1_3_2	1,031272354
5	_R1_HOM1_3_4	0,4
6	_R2_HOMSTY_3_1	0,408197074
7	_R2_HOMSTY_3_2	0,4
8	_R2_HOMSTY_3_4	0,4
9	_R2_HOM1_3_1	0,4
10	_R2_HOM1_3_2	1,096481502
11	_R2_HOM1_3_4	0,4
12	_R3_HOMSTY_3_1	0,738890995
13	_R3_HOMSTY_3_2	0,4
14	_R3_HOMSTY_3_4	0,4
15	_R3_HOM1_3_1	0,4
16	_R3_HOM1_3_2	0,968944711
17	_R3_HOM1_3_4	0,470371556
18	_R4_HOMSTY_3_1	0,609791644
19	_R4_HOMSTY_3_2	0,4
20	_R4_HOMSTY_3_4	0,4
21	_R4_HOM1_3_1	0,4
22	_R4_HOM1_3_2	0,998656614
23	_R4_HOM1_3_4	0,465830822
24	_R5_HOMSTY_3_1	0,743507517
25	_R5_HOMSTY_3_2	0,406364241
26	_R5_HOMSTY_3_4	0,4
27	_R5_HOM1_3_1	0,4
28	_R5_HOM1_3_2	0,97919137
29	_R5_HOM1_3_4	0,496159837
30	_R6_HOMSTY_3_1	0,421884952
31	_R6_HOMSTY_3_2	0,4
32	_R6_HOMSTY_3_4	0,4
33	_R6_HOM1_3_1	0,4
34	_R6_HOM1_3_2	1,095987273
35	_R6_HOM1_3_4	0,4
36	_R7_HOMSTY_3_1	0,4
37	_R7_HOMSTY_3_2	0,4
38	_R7_HOMSTY_3_4	0,4
39	_R7_HOM1_3_1	0,4
40	_R7_HOM1_3_2	1,033261722
41	_R7_HOM1_3_4	0,4

Figure 56 Values of design variables at convergence

Note that the variable names in Figure 56 are built with the following rules:

- variables starting with R_i are related to super-stringer number i
- variables $R^*_HOM^*$ are ply thicknesses for the *skin*
- variables $R^*_HOMSTY^*$ are ply thicknesses for the *stringers*
- the last digit is related to ply orientation (1 for 0° , 2 for 45° and 4 for 90°)

Furthermore, since a symmetry is assumed between 45° and -45° plies, the values $R^*_HOM_1_3_2$ and $R^*_HOMSTY_3_2$ have to be multiplied by two when considering total thickness.

Figure 57 shows the same results, but aggregated at the level of skin panels and stringers.

Total thicknesses	
Stringer 1	1,6
Skin panel 1	2,862544708
Stringer 2	1,608197074
Skin panel 2	2,992963004
Stringer 3	1,938890995
Skin panel 3	2,808260978
Stringer 4	1,809791644
Skin panel 4	2,86314405
Stringer 5	1,956236
Skin panel 5	2,854542576
Stringer 6	1,621884952
Skin panel 6	2,991974547

Figure 57 Values of design variables at convergence

IX. Summary & conclusions

Presented in this chapter is a flexible and robust approach to structural sizing optimization at different stages of product design maturity.

For early sizing stages a rapid sizing approach has been proposed, based on efficient neural network regression of local optimization results. These neural networks can be used either in the STIFFOPT tool for quick automated sizing of a full structure cover or can be interrogated to give optimum design results at structural element level. Improvements have been applied to the neural net construction and the Design of Experiments in order to obtain more robust results and to consider higher dimensions of the input space.

For preliminary sizing stages, all local optimizations are performed in the frame of the sizing process, evoking specialized tools in a two-level process with two systems of iterations. A PC cluster has been used for computational efficiency. The proposed approach is particularly suited to parallelization because all optimizations are independent from each other.

For detailed sizing stages a new optimization process was put in place at local level, considering nonlinear finite element analysis to evaluate the post-buckling behaviour of each panel. An original hybrid formulation was adopted to formulate the optimization problem, combining together linear buckling for skin buckling on-set and non-linear analysis for panel collapse. To solve the optimization problem, semi-analytical sensitivities were developed and embedded in a gradient-based optimization process. The efficiency and robustness of the full optimization process was demonstrated. This work is one of the few examples showing an accurate gradient-based optimization processes applied to non-linear finite element analysis. In this third sizing stage, the need for HPC is even greater, considering the long time necessary for each optimization (20 hours).

The implementation of the three sizing stages is to be completed in the near future. The same framework will be used for integration. A full multi-level optimization process will need to be developed controlling the overall optimality, that is, considering optimal load redistribution, design continuity and more general global constraints (such as stiffness constraints). The optimization process will have to be properly decomposed and coordinated and implemented based on HPC architectures (massive parallelism). The extended enterprise context is also to be considered with a structural design distributed around the world to different partners.^{35,36} All these different areas of investigation are being pursued in a recently started European Project named MAAXIMUS and focused on virtual design and testing of a composite fuselage.³⁷

References

- ¹Schmit, L.A., Mallet, R.H., “Structural synthesis and design parameter hierarchy”, Proceedings of the 3rd ASCE Conference on Electronic Computation, 1963, pp 269-300
- ²SAMTECH , “BOSS Quattro user’s handbook – Release 6.0-02”, 2008
- ³Remouchamps, A., Radovic, Y., “BOSS Quattro: an open system for parametric design”, Structural & Multidisciplinary Optimization , vol.23, pp. 140-152, 2002.
- ⁴Remouchamps, A., Grihon, S., Raick, C., Colson, B., Bruyneel, M., “BOSS Quattro: an open system for parametric design”, Structural & Multidisciplinary Optimization , vol.23, pp. 140-152, 2002.
- ⁵Schmit, L.A.Jr., Ramanathan R.K., “Multilevel Approach to Minimum Weight Design including Buckling Constraints” AIAA Journal 16(2),1978
- ⁶Balling, R.J., Sobieszczanski-Sobieski J., “An Algorithm for solving the System-level Problem in Multi-Level Optimization” NASA Contractor Report 195015, 1994
- ⁷Timoshenko, S., Gere E., “Theory of elastic stability” McGraw-Hill Book Co., 1936 (réimpr. 1963), 542 p
- ⁸MSC.Software, “NASTRAN Linear Static Analysis User’s Guide”, 2000
- ⁹AIRBUS France, « MTS004 : Manuel de calcul statique pour matériaux métalliques » , 2000
- ¹⁰“Numerical Algorithms Group – FORTRAN Library”, www.nag.co.uk
- ¹¹Fleury, C., “Dual methods for convex separable problems”, in Optimization of Large Structural Systems, Volume I (G.I.N Rozvany, editor), Kluwer Academic Publishers, The Netherlands, 1993, pp.509-530
- ¹²Bruyneel, M., Duysinx, P., Fleury, C., “A family of MMA approximations for structural optimization”, Structural & Multidisciplinary Optimization, vol.24, pp.263-276, 2002.
- ¹³MSC.Software, “PATRAN Programming Command Language Users Guide”, 2000
- ¹⁴Vaswani, Vikram, “PHP Programming Solutions” Mc Graw-Hill. ISBN 0-07-148745-X
- ¹⁵“PHP - Hypertext Processor” anonymous, <http://www.php.net/>, accessed March 2008
- ¹⁶Merval, A., Samuelides, M., Grihon, S., “Application of Response Surface methodology to stiffened panel optimization” 47th conference on AIAA/ASME/ASCE/AHS/ASC Structures, Structural Dynamics & Material Conference, 2006
- ¹⁷Simpson, T.W., Mauery T.M., Korte, J.J., Mistree,F., ”Comparison of Response

Surfaces and Kriging Models for Multidisciplinary Design Optimization”, AIAA paper 98-4755, 1998

¹⁸Sellar, R.S., Batill, S.M., Renaud, J.E., “Response Surface Based Concurrent Subspace Optimization for Multidisciplinary System Design” AIAA paper, 1996

¹⁹Bishop, C.M., “Neural Networks for Pattern Recognition” Clarendon Press, Oxford, 1997.

²⁰Dreyfus, G., Samuelides, M., Gordon, M., “Réseaux de Neurones: Méthodologie et applications”, Eyrolles ed., Paris, 2002

²¹Jordan, M.I., Jacobs, R.A., Nowlan, S.J., Hinton, G.E., “Adaptive Mixture of Local Experts”, 70-87 1991

²²Jordan, M.I, Jacobs R.A., “Hierarchical Mixtures of Experts and the EM Algorithm” Neural Computation, 6, 181-214, 1994.

²³Wang, G.G., “Adaptive Response Surface Method Using Inherited Latin Hypercube Design Points” Transaction of the ASME, Journal of Mechanical Design, Vol.125, pp.210-220, June 2003

²⁴Cohn, D.A., “Neural Network Exploration using Optimal Experimental Design”, MIT CBCL paper N°99, 1994

²⁵The Mathworks, “MATLAB User’s Guide – release R2008b – Neural Network toolbox,” 2008

²⁶Colson, B., Bruyneel, M., Grihon, S., Jetteur, P., Remouchamps, A., “Composite panel optimization with nonlinear finite element analysis and semi-analytical sensitivities”, NAFEMS Seminar – Simulating Composite Materials and Structures, November 6-7 Bad Kissingen, Germany, 2007

²⁷Remouchamps, A., Grihon, S., Raick, C., Colson, B., Bruyneel, M., “Numerical Optimization : a design space odyssey” International Workshop, 2007: Advancements in Design Optimization of Materials, Structures and mechanical Systems, 17-20 December 2007, Xi’an China

²⁸SAMTECH, “SAMCEF: Software package for finite element analysis of structures,” S.A., Liège Belgium, www.samcef.com

²⁹Lanzi, L., Giavotto, V., “Post-buckling optimization of composite stiffened panels: computations and experiments” Composite Structures, vol.73, pp.208-2030,2006

³⁰Bruyneel, M., “A general and effective approach for the optimal design of fibres reinforced composite structures” Composites Science & Technology, vol.66, pp. 1303,1314, 2006

³¹Grihon, S., Michel, L., Barrau, J.J., “Buckling optimization of composite panels via lay

up tables” IIIrd European Conference on Computational Mechanics Solids, Structures and Coupled Problems in Engineering, Lisbon (Portugal) 2006

³²Carpentier, A., Michel, L., Grihon, S., Barrau, J.J., “Optimization Methodology of Composite Panels” IVth European Conference on Computational Mechanics Solids, Structures and Coupled Problems in Engineering, Biarritz (France) 2007

³³Riks, E., Rankin, C., Brogan, F., “On the solution of mode jumping phenomena in thin walled shell structures”, *Comp.Meth.Appl.Mech.Engng.vol.136*, pp 59-92, 1996

³⁴Bruyneel, M., Colson, B., Remouchamps, A., “Discussion on some convergence problems in buckling optimization”, *Structural & Multidisciplinary Optimization*, vol.35, pp.181-186, 2008

³⁵Merval, A., Samuelidès, M., Grihon, S., “Multi-level Optimization with local mass minimization” 2nd European Conference for Aerospace Sciences – EUCASS 2007

³⁶Merval, A., Samuelidès, M., Grihon, S., “Lagrange Kuhn-Tucker Coordination for Multilevel sizing of Aeronautical Structures”, 49th conference on AIAA/ASME/ASCE/AHS/ASC Structures, Structural Dynamics & Material Conference, 2008

³⁷“MAAXIMUS” Integrated Project, 7th Framework, 2008-2013